A damage-plasticity framework for fluid-infiltrating geomaterials with size-dependent anisotropy

WaiChing "Steve" Sun
Assistant Professor
Department of Civil Engineering and Engineering Mechanics,
Fu Foundation School of Engineering and Applied Science,
Columbia University, New York, USA.

Acknowledgement of Current and Former Research Group Members

Kun Wang

Hyoung Suk Suh

Nikolaos Vlassis

Eric Cushman Bryant

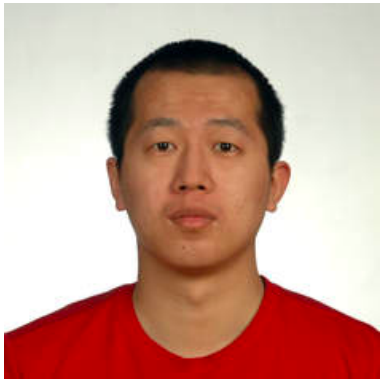

Ran Ma, PhD

Yousef Heider, PhD

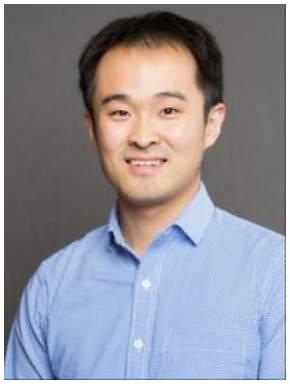

Chanuqi Liu, PhD

Jinhyun Choo, PhD, now HKU

Yang Liu, PhD, now Northeastern

SeonHong Na, PhD, now McMaster

Brittle-ductile transition

0.1 MPa 49 MPa 98 MPa 147 MPa

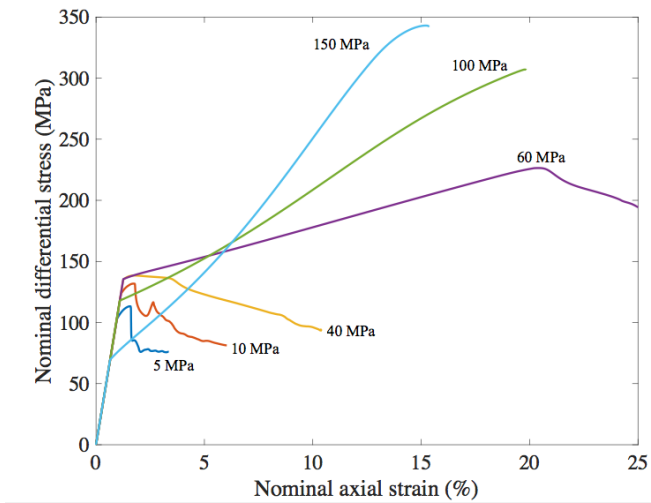

- Brittle regime - fracture with small scale yielding
- Quasi-brittle regime - fracture with softening
- Ductile regime - plasticity + fracture

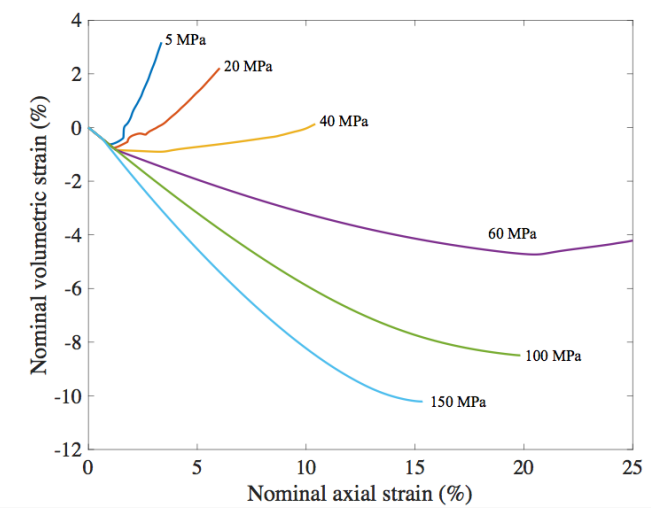

Choo & Sun, CMAME 2018

Example 1: Evolving cracks and anti-crack filled with pore fluid

Background

- Common strategies
  - Cohesive zone interface element (on DG or standard FEM)

    Fracture process zone, known crack path
  - X-FEM & Assumed Strain

    Powerful and accurate approach to model problems exhibiting discontinuities and inhomogeneities, difficulty in modeling crack branching and curved crack path
  - Phase-field

    Fracture surface is approximated by a phase-field.

    need fine mesh to improve convergence and geometrically represent the fracture
  - Element erosion (deletion)

    Simple scheme, spurious mesh dependency
  - Meshless method

    Not need to embed strong discontinuities but need to recover geometrical features via implicit function (e.g. level set)

Other possibility – peridynamic, lattice-spring, lattice-beam models

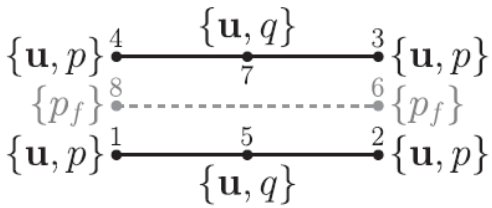

Zero-thickness interface element with hydro-mechanical coupling

e.g. Carrier, Benoit, and Sylvie Granet (2012)

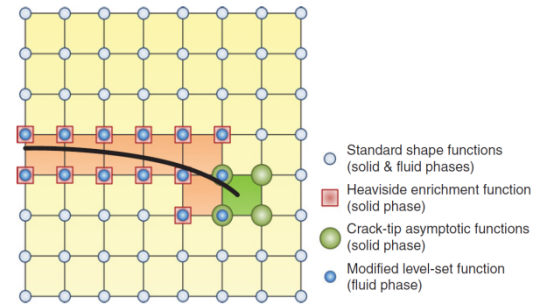

Figure 10.16 The enriched nodal points of the displacement and pressure fields in porous media

e.g. Khoei, Amir R. Extended Finite Element Method: Theory and Applications

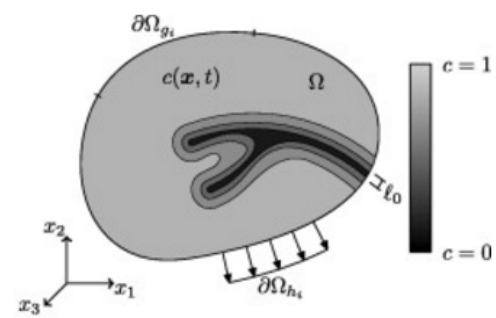

e.g. Borden, Michael J., et al. (2012)

Compaction band as Mode I anti-crack

Compaction band in Bentheim sandstone
(UPPER LEFT, Baud et al. 2004,
LOWER, Stanchits et al. 2009)

Compaction band in Navajo sandstone
(RIGHT, Fossen et al. 2011)

Compaction bands have been idealized as anti-cracks (cf. Sternolf & Pollard 2002 and Rudnicki 2007) and the associated energy release rate has been measured experimentally (e.g. Stanchits et al. 2009).

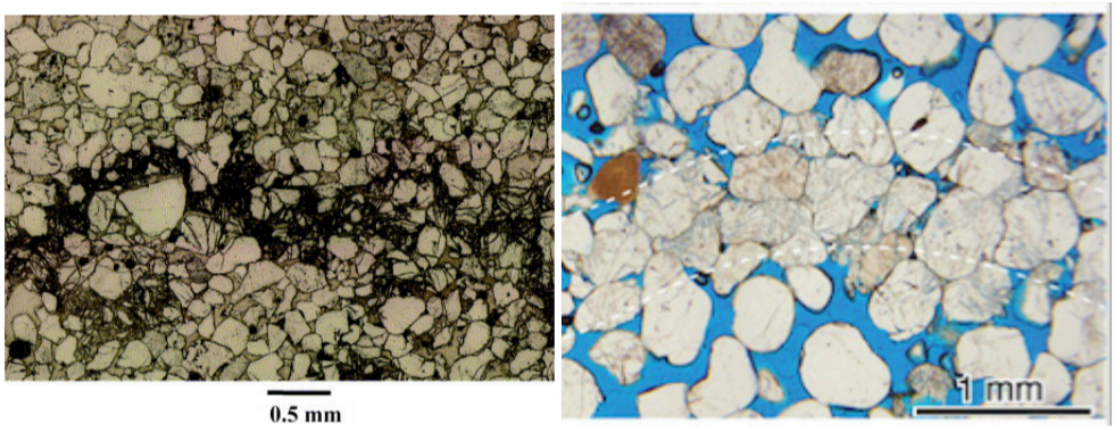

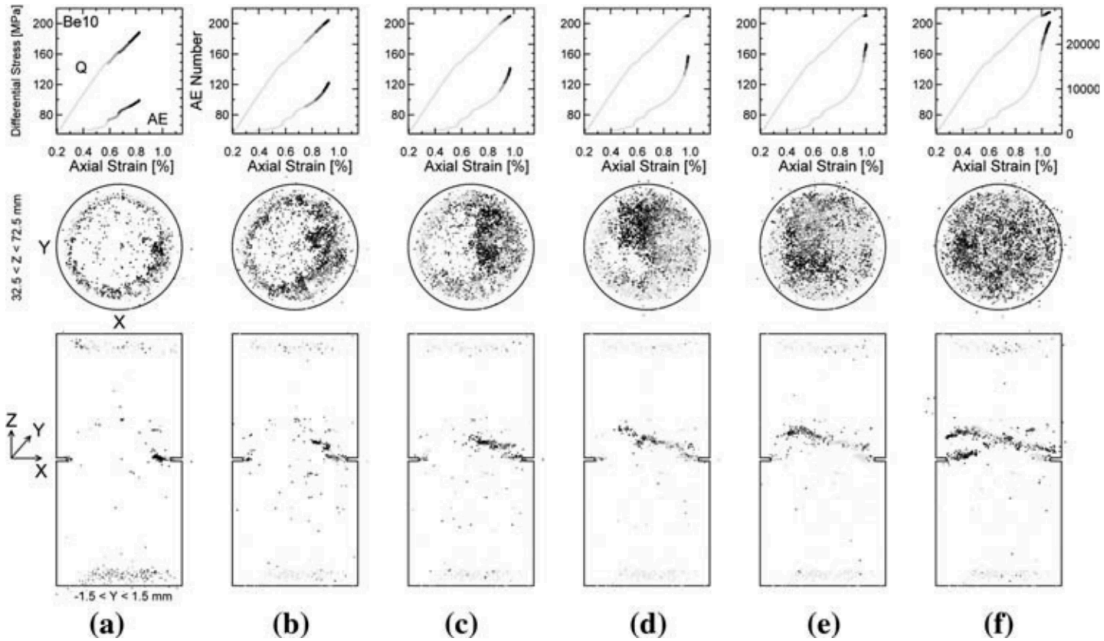

Eigen-erosion approach

- Simple implementation
  - Able to capture curved crack path, crack branching, coalescence
  - Mesh independent
  - Robust
- Eigen-fracture (Schmidt et al. 2009)
  - Eigen-fracture energy functional:

$$F_\epsilon(u, \varepsilon^*, t) = \int_\Omega W(\varepsilon(u) - \varepsilon^*)\,\mathrm{d}V - \int_{\Gamma_2} \bar{T} \cdot u\,\mathrm{d}S + \underline{G_c \frac{|C_\epsilon|}{2\epsilon}}$$

Regularized fracture energy term

  - Phase field energy functional:

$$F_\epsilon(u, \varphi, t) = \int_\Omega W(\varepsilon(u), \varphi)\, dV - \int_{\Gamma_2} \bar{T} \cdot u\, dS + \underline{\int_\Omega G_c\left(\frac{1}{2\epsilon}\|1 - \varphi\|^2 + \frac{\epsilon}{2}\|\nabla\varphi\|^2\right) dV}$$

- Eigen-erosion (Pandolfi and Ortiz. 2012)
  - Restrict Eigen-deformation to binary case: either intact or completely failed
  - For FEM: leads to element erosion scheme that is mesh-independent

Formulation of variational eigen-erosion in fluid-saturated porous media

Free Energy functionals

$$W(\boldsymbol{\varepsilon}, \boldsymbol{\varepsilon}^*, p^f) = W_{eff}(\boldsymbol{\varepsilon}, \boldsymbol{\varepsilon}^*) + W_{fluid}(\boldsymbol{\varepsilon}, p^f)$$

$$W_{\text{eff}}(\boldsymbol{\varepsilon}, \boldsymbol{\varepsilon}^*) = \int_\Omega \frac{1}{2}(\boldsymbol{\varepsilon} - \boldsymbol{\varepsilon}^*) : \boldsymbol{\mathcal{C}}^e : (\boldsymbol{\varepsilon} - \boldsymbol{\varepsilon}^*) dV \quad W_{\text{fluid}}(\boldsymbol{\varepsilon}, p^f) = \frac{M}{2}[(1-b)\varepsilon_v - \frac{p^f}{M}]^2$$

with eigen-deformation corresponding to fracture (set C) and compaction band (set CB)

$$\boldsymbol{\varepsilon}^*(\boldsymbol{x}, t) = \begin{cases} \boldsymbol{\varepsilon}(\boldsymbol{x}, t) & \boldsymbol{x} \in C \\ \varepsilon_{\text{inel}} \boldsymbol{n}_{CB}(\boldsymbol{x}, t) \otimes \boldsymbol{n}_{CB}(\boldsymbol{x}, t) & \boldsymbol{x} \in CB \\ \boldsymbol{0} & \boldsymbol{x} \in \Omega \setminus (C \cup CB) \end{cases}$$

C: Crack set
CB: Compaction Band set
Intact element

Fluid dissipation

$$\mathcal{D}_f(\boldsymbol{\varepsilon}, \boldsymbol{\varepsilon}^*, p^f) = -\int_0^t [\int_\Omega \frac{1}{2} \frac{\boldsymbol{\kappa}(\boldsymbol{\varepsilon}, \boldsymbol{\varepsilon}^*, p^f)}{\mu} : (\nabla p^f \otimes \nabla p^f) dV] d\tau$$

Enhanced or suppressed permeability due to fracture and compaction band

Variational Statement of the variational eigen-erosion in fluid-saturated porous media

Find :the saddle point of the Energy-dissipation Functional with respect to solid displacement and pore pressure

$$
\begin{aligned}
F_{(\epsilon_C,\epsilon_{CB})}(\boldsymbol{\varepsilon},\boldsymbol{\varepsilon}^*,p^f,t) = & \int_\Omega \frac{1}{2}(\boldsymbol{\varepsilon}-\boldsymbol{\varepsilon}^*):\mathcal{C}^e:(\boldsymbol{\varepsilon}-\boldsymbol{\varepsilon}^*)dV - \int_{\Gamma_t}\bar{\boldsymbol{T}}\cdot\boldsymbol{u}dS \\
& + \int_\Omega \frac{M}{2}[(1-b)\varepsilon_v - \frac{p^f}{M}]^2 dV + \int_0^t [\int_\Omega \bar{\boldsymbol{s}}\cdot p^f dV - \int_{\Gamma_q}\bar{\boldsymbol{q}}\cdot p^f dS]d\tau \\
& + G_C\frac{|C_{\epsilon_C}|}{2\epsilon_C} + G_{CB}\frac{|C_{\epsilon_{CB}}|}{2\epsilon_{CB}} + \mathcal{D}_f(\boldsymbol{\varepsilon},\boldsymbol{\varepsilon}^*,p^f).
\end{aligned}
$$

Subjected to a monotonicity constraint that enforces history-dependence

$$
\begin{cases} C(t)\subset C(t+\Delta t) \\ CB(t)\subset CB(t+\Delta t) \end{cases}
\qquad
\boldsymbol{\varepsilon}^*(\boldsymbol{x},t) = \begin{cases} \boldsymbol{\varepsilon}(\boldsymbol{x},t) & \boldsymbol{x}\in C \\ \varepsilon_{\text{inel}}\boldsymbol{n}_{CB}(\boldsymbol{x},t)\otimes\boldsymbol{n}_{CB}(\boldsymbol{x},t) & \boldsymbol{x}\in CB \\ \boldsymbol{0} & \boldsymbol{x}\in\Omega\setminus(C\cup CB) \end{cases}
$$

Wang & Sun, CMAME, 2017

Departure from classical element deletion method – Non-locality from crack neighborhood

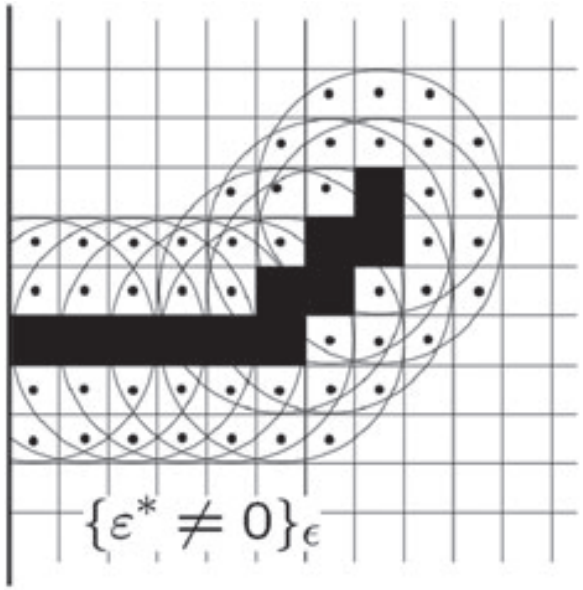

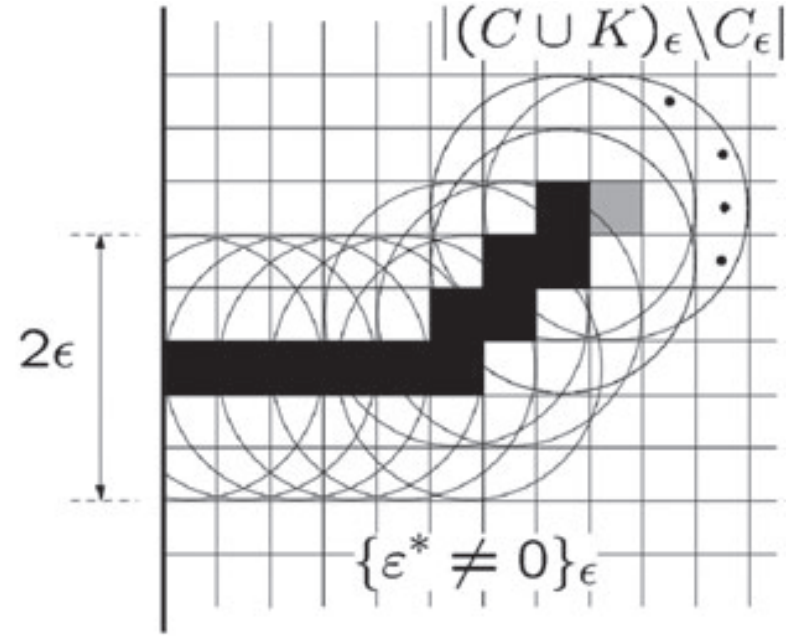

Crack set and intact element in epsilon neighborhood

Crack set in the epsilon neighborhood

$$\Delta A_K = \frac{|(C \cup K)_\epsilon \backslash C_\epsilon|}{2\epsilon}$$

Crack area increment

Pandolfi, Anna, and Michael Ortiz. (2012)

Mechanical vs. Hydraulic Aperture

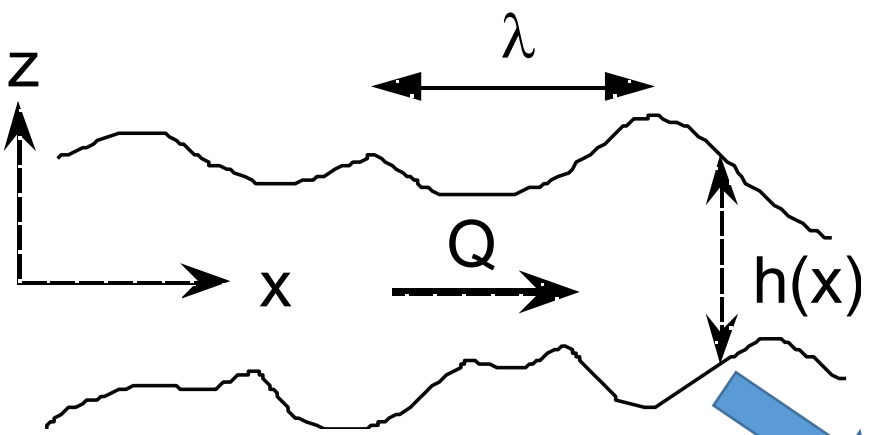

Mechanical aperture

Navier-Stokes Equations

↓ Ignore Inertia Terms

Stokes Equations

↓ Ignore Out-of-Plane Velocity

Reynolds Lubrication Equation

↓ Effective Medium Methods

Cubic Law

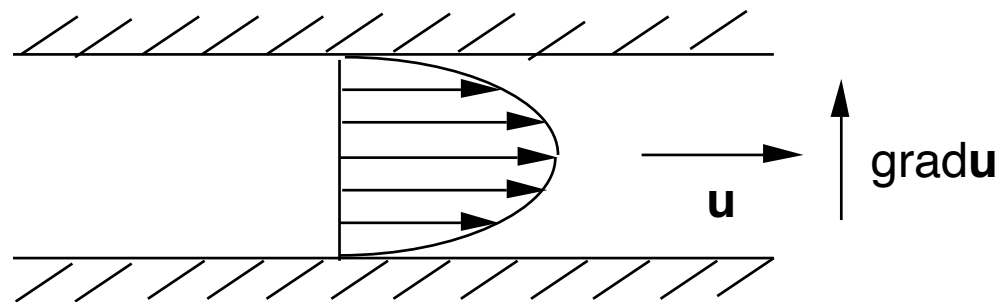

Hydraulic aperture

Figures from Robert Zimmerman

Effect of flow conduit created by cracks

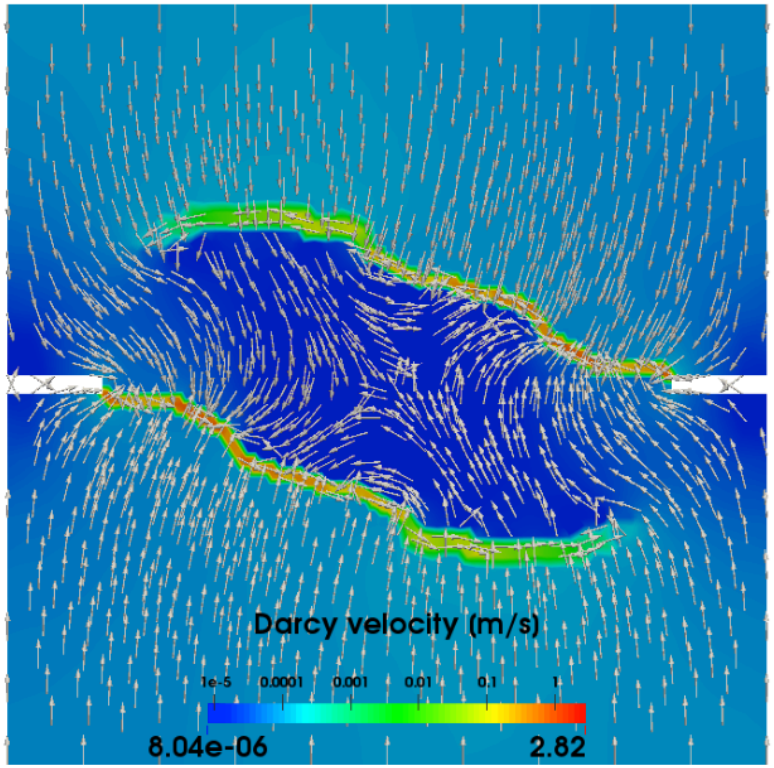

strain rate $0.0005\ s^{-1}$

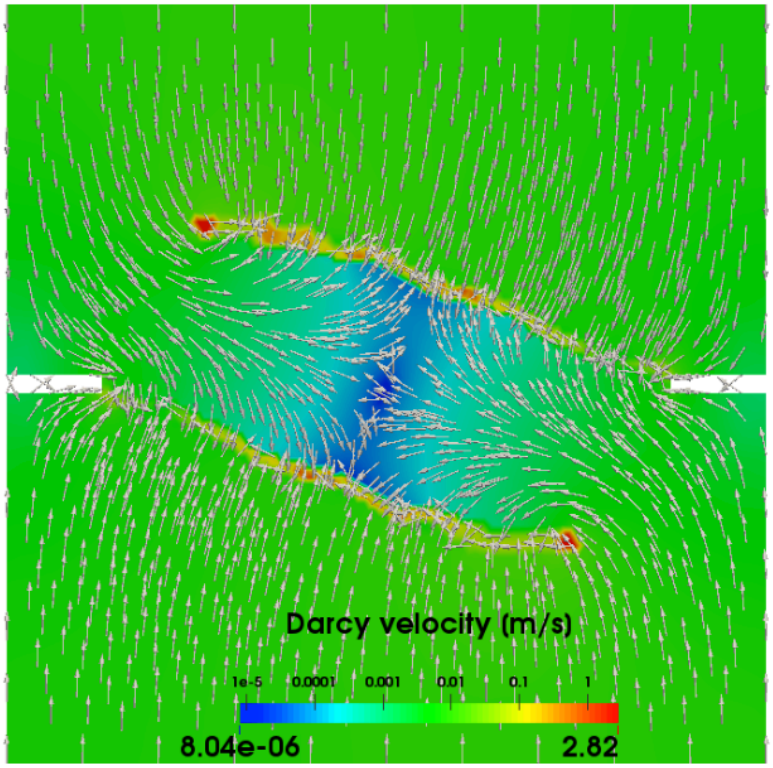

strain rate $0.05\ s^{-1}$

Test 1: Shear loading Ps = 50MPa, 0.05s-1
Vertical strain rate = 0.0005s-1

Example: Compaction band as flow Barrier

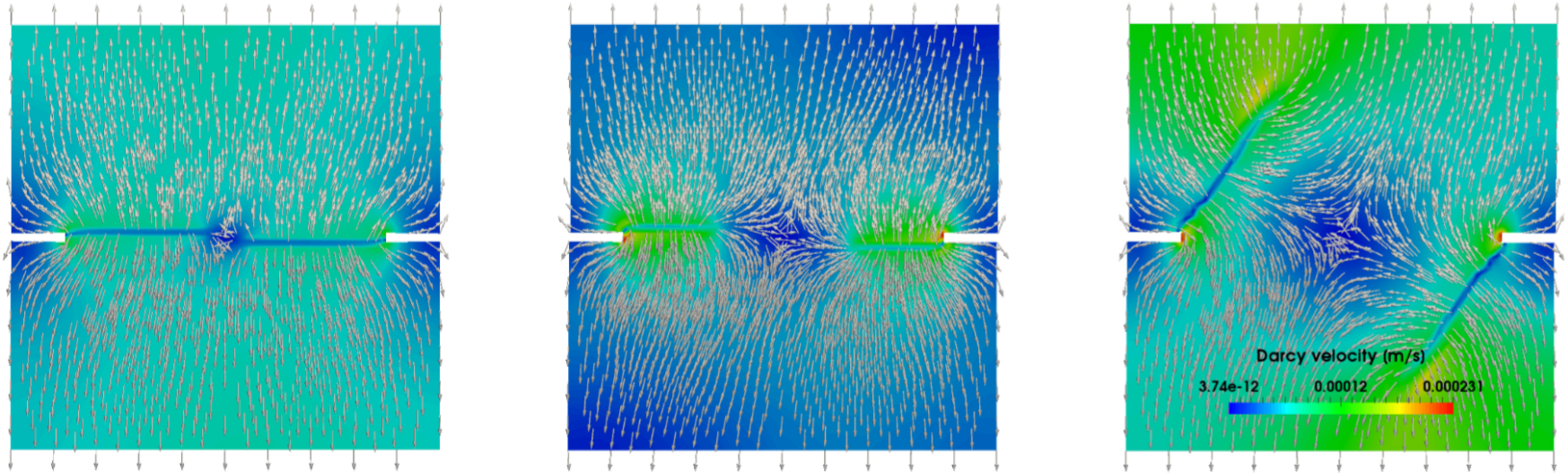

(a) $P_s = 50$ MPa **(b)** $P_s = 100$ MPa **(c)** $P_s = 120$ MPa

Example: Crack propagation and coalescence in heterogeneous porous media

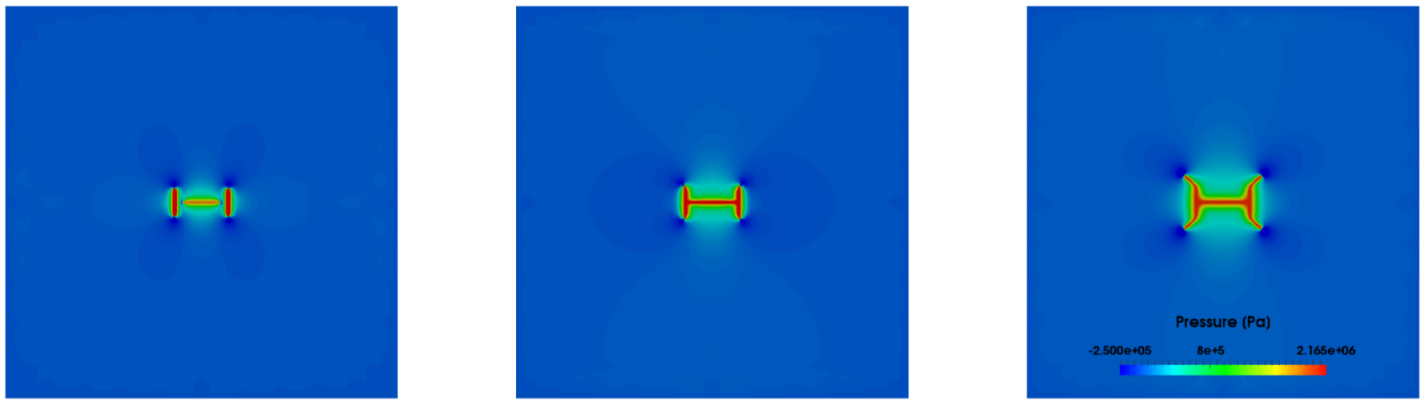

(a) t = 2 s **(b)** t = 3 s **(c)** t = 5 s

Fig. 21: Fluid driven propagation and coalescence of fractures in homogeneous porosity field. $v_{\text{inject}} = 0.00025$ m/s. Fluid pressure at t = 2 s, 3 s, 5 s.

Wang & Sun, CMAME, 2017.

Phase field version: Wick & Wheeler, SPE, 2014

Example: Effect of injection rate in heterogeneous porous media

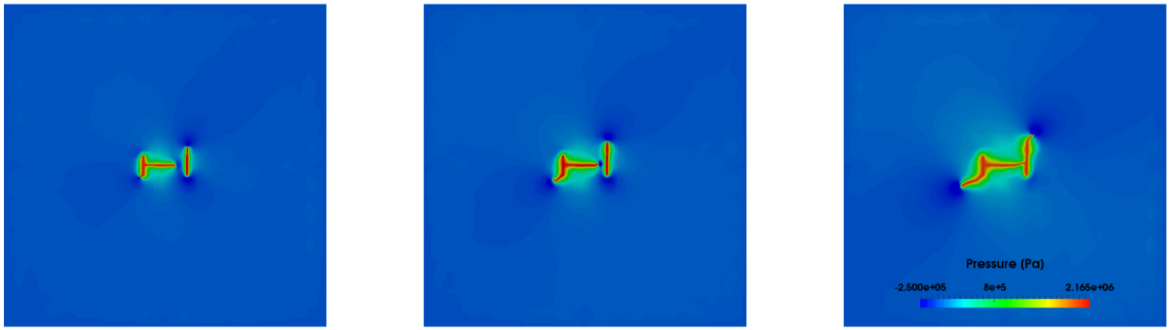

(a) t = 2 s **(b)** t = 3 s **(c)** t = 5 s

Fig. 22: Fluid driven propagation and coalescence of fractures in heterogeneous porosity field. $v_{\text{inject}} = 0.00025$ m/s. Fluid pressure at t = 2 s, 3 s, 5 s.

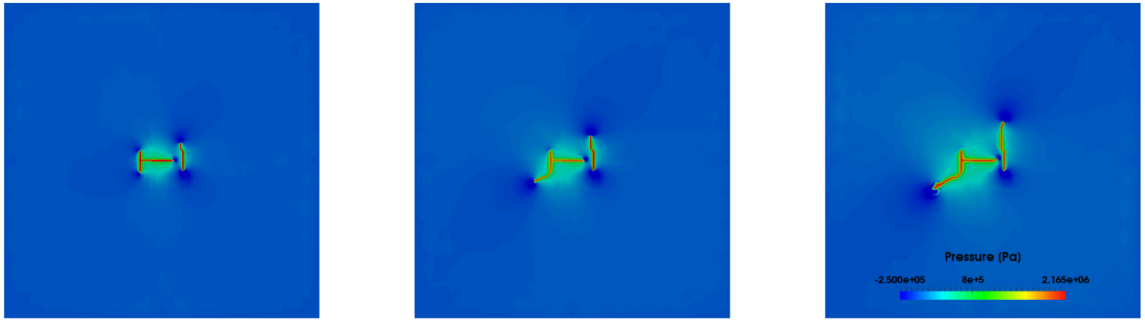

(a) t = 0.2 s **(b)** t = 0.3 s **(c)** t = 0.5 s

Fig. 23: Fluid driven propagation and coalescence of fractures in heterogeneous porosity field. $v_{\text{inject}} = 0.0025$ m/s. Fluid pressure at t = 0.2 s, 0.3 s, 0.5 s.

Wang & Sun, CMAME 2017.

Anisotropic materials in the ductile regime

Motivation

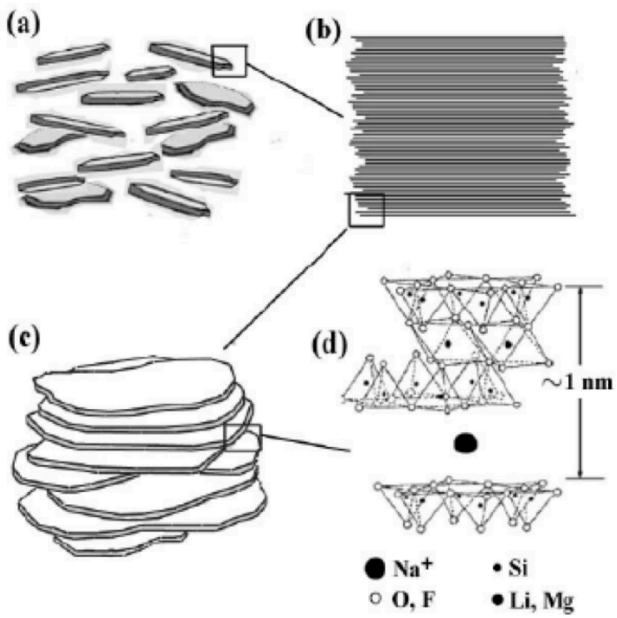

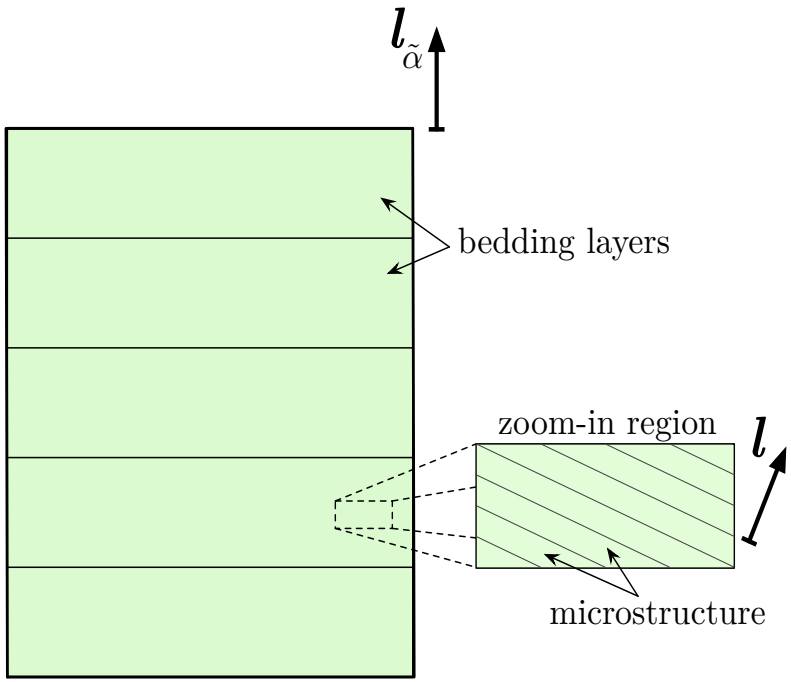

Bryant & Sun, CMAME 2019

Size-dependent anisotropy

- Goal: Introduce different "effective" anisotropy or different size of specimen numerically

- Strategy:

Critical State Plasticity → Semnani et al. 2016 → Anisotropic Critical State Plasticity → Introduce anisotropic regularization (this work) → Anisotropic Gradient Plasticity

Review on Anisotropic Cam-clay model

Anisotropic Elasticity

$$W(\boldsymbol{\epsilon}^{\mathrm{e}}, \boldsymbol{\alpha}, \tilde{\boldsymbol{\alpha}}) = W^{\mathrm{e}}(\boldsymbol{\epsilon}^{\mathrm{e}}) + W^{\mathrm{p}}(\boldsymbol{\alpha}, \tilde{\boldsymbol{\alpha}}).$$

where $W^{\mathrm{e}} = \frac{1}{2}\boldsymbol{\epsilon}^{\mathrm{e}} : \boldsymbol{C}^{\mathrm{e}} : \boldsymbol{\epsilon}^{\mathrm{e}}.$ and $\boldsymbol{C}^{\mathrm{e}} = c_1\boldsymbol{E}_1 + c_2\boldsymbol{E}_2 + c_3(\boldsymbol{E}_3 + \boldsymbol{E}_4) + c_5\boldsymbol{F} + c_6\boldsymbol{G}$

The key idea is to introduce p^* and q^* as weighted norms to simplify implementation

$$p^* = \boldsymbol{a}_p : \boldsymbol{\sigma}, \quad q^* = \sqrt{\frac{1}{2}\boldsymbol{\sigma} : \boldsymbol{A}_q : \boldsymbol{\sigma}},$$

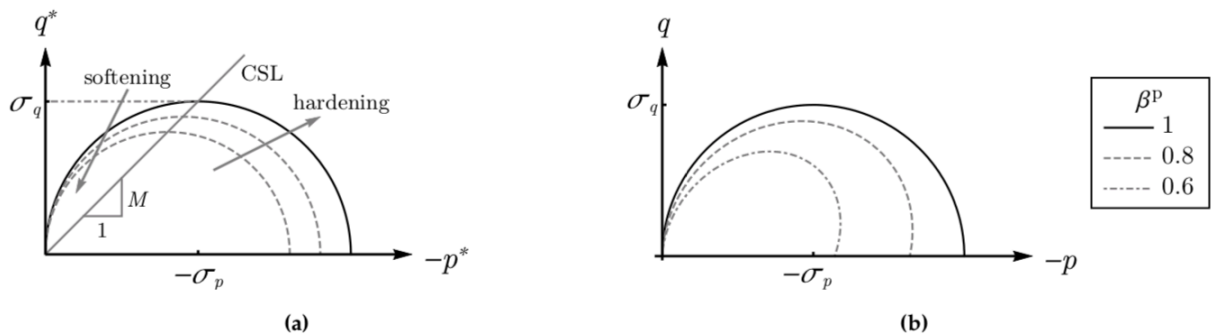

Fig. 1: Geometric interpretation of the mapped two-invariant yield criterion, Eq. (34): (a) introducing M as the slope of the critical state line (CSL) in the starred scalar space, after Ortiz and Pandolfi [2004], and with softening and hardening trends after Borja [2013]; and, (b) unmapped two-invariant yield criterion parameterized by the mapping coefficient, varying $\beta^{\mathrm{dev}} = \beta^{\mathrm{vol}}$ at fixed $\alpha^{\mathrm{dev}} = \alpha^{\mathrm{vol}} = \gamma^{\mathrm{dev}} = \gamma^{\mathrm{vol}} = 1$, after Semnani et al. [2016].

Anisotropic gradient regularization

Two additional energy functionals are added to introduce gradient dependence on the plastic work

$$W^{\mathrm{p}}_{\tilde{\boldsymbol{\alpha}}}(\boldsymbol{\alpha}, \tilde{\boldsymbol{\alpha}}) = \overbrace{\frac{k_\lambda}{2}\left(\tilde{\lambda} - \lambda\right)^2 + \frac{k_v}{2}\left(\tilde{\epsilon}^{\mathrm{p}}_v - \epsilon^{\mathrm{p}}_v\right)^2}^{\text{penalty functional terms}} + \overbrace{\frac{K_\lambda l_\lambda^2}{2}\nabla\tilde{\lambda}\cdot\boldsymbol{\omega}_\lambda\cdot\nabla\tilde{\lambda} + \frac{K_v l_v^2}{2}\nabla\tilde{\epsilon}^{\mathrm{p}}_v\cdot\boldsymbol{\omega}_v\cdot\nabla\tilde{\epsilon}^{\mathrm{p}}_v}^{\text{regulzarization functional terms}},$$

where the structural tensor for the anisotropic regularization is

$$\boldsymbol{\omega}_\lambda = (\boldsymbol{p}_\lambda \otimes \boldsymbol{p}_\lambda) : \mathbf{1} = \mathbf{1} + \phi_\lambda \boldsymbol{\phi}_\lambda + \chi_\lambda \boldsymbol{\chi}_\lambda, \quad \boldsymbol{p}_\lambda = \boldsymbol{\phi}_\lambda\sqrt{1+\phi_\lambda} + \boldsymbol{\chi}_\lambda\sqrt{1+\chi_\lambda},$$

Anisotropic gradient regularization

Incremental update are obtained from Euler-Lagrange equation of the incremental energy functional, i.e.,

$$\zeta_{\,n+1} = \arg\min_{\zeta_{\,n+1}} W(\zeta_{\,n+1}), \qquad \zeta_{\,n+1} = \{\boldsymbol{\epsilon}^{\mathrm{e}}_{n+1}, \tilde{\lambda}_{n+1}, \tilde{\epsilon}^{\mathrm{p}}_{v\;n+1}\},$$

which leads to

Local governing equation for constitutive laws

$$\frac{\delta W(\zeta_{\,n+1})}{\delta \boldsymbol{\epsilon}^{\mathrm{e}}_{n+1}} = \overbrace{\boldsymbol{\sigma}_{n+1} - \sigma_{q\;n+1}\frac{\partial \Delta\lambda}{\partial \Delta\boldsymbol{\epsilon}^{\mathrm{p}}} - \sigma_{p\;n+1}\boldsymbol{b}_v}^{\text{purely local terms}}$$

$$\overbrace{+\,k_\lambda\left(\tilde{\lambda}_{n+1} - \lambda_{n+1}\right)\frac{\partial \Delta\lambda}{\partial \Delta\boldsymbol{\epsilon}^{\mathrm{p}}} + k_v\left(\tilde{\epsilon}^{\mathrm{p}}_{v\;n+1} - \epsilon^{\mathrm{p}}_{v\;n+1}\right)\boldsymbol{b}_v}^{\text{micromorphic terms}} = \mathbf{0},$$

Regularized modified Helmholtz equations

$$\frac{\delta W(\zeta_{\,n+1})}{\delta \tilde{\lambda}_{n+1}} = k_\lambda(\tilde{\lambda}_{n+1} - \lambda_{n+1}) - K_\lambda l_\lambda^2\,\nabla\cdot(\boldsymbol{\omega}_\lambda \cdot \nabla\,\tilde{\lambda}_{n+1}) = 0, \text{ in } \mathcal{B},$$

$$\frac{\delta W(\zeta_{\,n+1})}{\delta \tilde{\epsilon}^{\mathrm{p}}_{v\;n+1}} = k_v(\tilde{\epsilon}^{\mathrm{p}}_{v\;n+1} - \epsilon^{\mathrm{p}}_{v\;n+1}) - K_v l_v^2\,\nabla\cdot(\boldsymbol{\omega}_v \cdot \nabla\,\tilde{\epsilon}^{\mathrm{p}}_{v\;n+1}) = 0, \text{ in } \mathcal{B},$$

Special case: Isotropic gradient regularization

- Nonlocal Modified Cam-Clay (MCC) model
  - Yield function (cf. Borja, 2013)

$$f_y = \frac{q^2}{M^2} + p'(p' - p'_c) = 0$$

where $p' = \frac{1}{r}\mathrm{tr}(\boldsymbol{\sigma}'), \quad q = \sqrt{\frac{2}{3}} \parallel \boldsymbol{s} \parallel, \quad \boldsymbol{s} = \boldsymbol{\sigma}' - p'\mathbf{1}$

  - Hardening

$$\dot{p}'_c = -\frac{\dot{\varepsilon}^p_v}{c_c - c_r} p'_c$$

(using the bilogarithmic relation between the specific volume and p'_c)

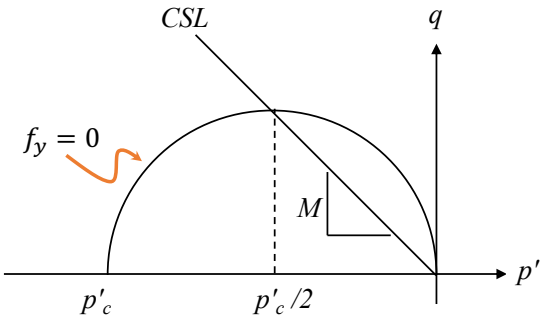

- The discrete hardening relation in a residual form

$$f_r = p'_c - p'_{c,old} \exp\left(\frac{\varepsilon^e_v - \varepsilon^{e\ \mathrm{trial}}_v}{c_c - c_r}\right) + \boxed{\epsilon_p(\bar{\alpha} - \alpha)} = 0$$

ϵ_p : penalty parameter
$\bar{\alpha} \equiv p_c{}'$: local internal variable
α : global micomorphic variable

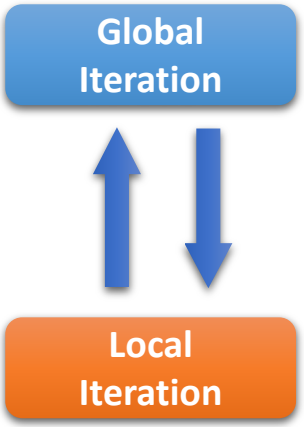

$$\begin{cases} \nabla \cdot (\boldsymbol{\sigma}' - p\mathbf{1}) + \rho \boldsymbol{g} = \mathbf{0} \\ \nabla \cdot \dot{\boldsymbol{u}} + \nabla \cdot \left(-\frac{1}{\rho_f g}\boldsymbol{k} \cdot \nabla p\right) = 0 \\ \alpha - l_p^2 \Delta\alpha = \bar{\alpha} \end{cases}$$

$$\boldsymbol{r} = \begin{Bmatrix} \varepsilon^e_v - \varepsilon^{e\ \mathrm{trial}}_v + \Delta\lambda \partial_{p'} f \\ \varepsilon^e_s - \varepsilon^{e\ \mathrm{trial}}_s + \Delta\lambda \partial_{q'} f \\ f_y \\ f_r \end{Bmatrix}; \quad \boldsymbol{x} = \begin{Bmatrix} \varepsilon^e_v \\ \varepsilon^e_s \\ \Delta\lambda \\ p'_c \end{Bmatrix};$$

Anisotropic gradient regularization

Incremental update are obtained from Euler-Lagrange equation of the incremental energy functional, i.e.,

$$\zeta_{\,n+1} = \arg\min_{\zeta_{\,n+1}} W(\zeta_{\,n+1}), \qquad \zeta_{\,n+1} = \{\boldsymbol{\epsilon}^{\mathrm{e}}_{n+1}, \tilde{\lambda}_{n+1}, \tilde{\epsilon}^{\mathrm{p}}_{v\;n+1}\},$$

which leads to

Local governing equation for constitutive laws

$$\frac{\delta W(\zeta_{\,n+1})}{\delta \boldsymbol{\epsilon}^{\mathrm{e}}_{n+1}} = \overbrace{\boldsymbol{\sigma}_{n+1} - \sigma_{q\;n+1}\frac{\partial \Delta\lambda}{\partial \Delta\boldsymbol{\epsilon}^{\mathrm{p}}} - \sigma_{p\;n+1}\boldsymbol{b}_v}^{\text{purely local terms}}$$

$$\overbrace{+\,k_\lambda\left(\tilde{\lambda}_{n+1} - \lambda_{n+1}\right)\frac{\partial \Delta\lambda}{\partial \Delta\boldsymbol{\epsilon}^{\mathrm{p}}} + k_v\left(\tilde{\epsilon}^{\mathrm{p}}_{v\;n+1} - \epsilon^{\mathrm{p}}_{v\;n+1}\right)\boldsymbol{b}_v}^{\text{micromorphic terms}} = \mathbf{0},$$

Regularized modified Helmholtz equations

$$\frac{\delta W(\zeta_{\,n+1})}{\delta \tilde{\lambda}_{n+1}} = k_\lambda(\tilde{\lambda}_{n+1} - \lambda_{n+1}) - K_\lambda l_\lambda^2\,\nabla\cdot(\boldsymbol{\omega}_\lambda \cdot \nabla\,\tilde{\lambda}_{n+1}) = 0, \text{ in } \mathcal{B},$$

$$\frac{\delta W(\zeta_{\,n+1})}{\delta \tilde{\epsilon}^{\mathrm{p}}_{v\;n+1}} = k_v(\tilde{\epsilon}^{\mathrm{p}}_{v\;n+1} - \epsilon^{\mathrm{p}}_{v\;n+1}) - K_v l_v^2\,\nabla\cdot(\boldsymbol{\omega}_v \cdot \nabla\,\tilde{\epsilon}^{\mathrm{p}}_{v\;n+1}) = 0, \text{ in } \mathcal{B},$$

Plastic Flow direction w/ increasing anisotropic regularization effect

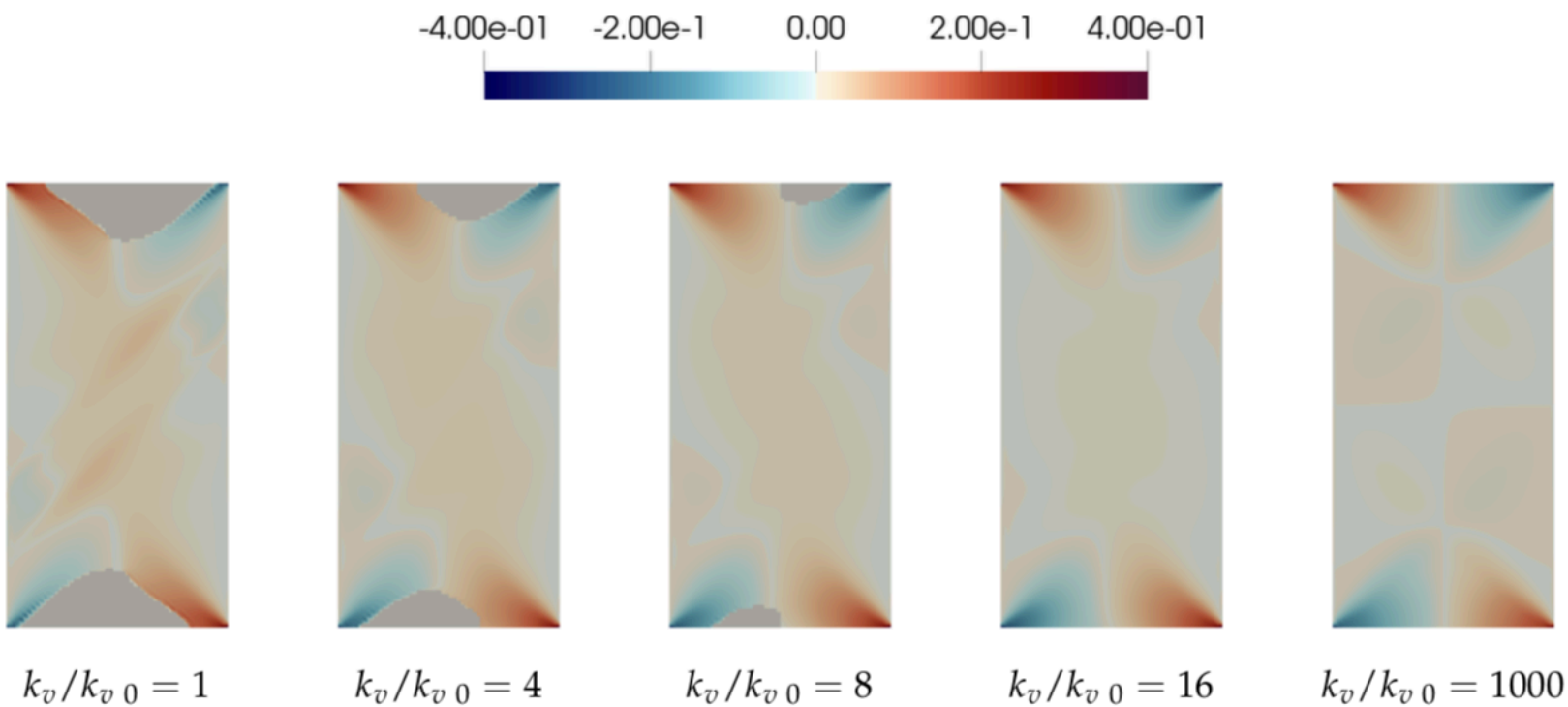

Fig. 12: Angle from horizontal of plastic strain's eigenvector corresponding to its greatest (most dilative) in-plane eigenvalue (in radians), for diffusively anisotropic plane strain compression case, with $\phi_v = 16$ and $\boldsymbol{l}_v$ described by $\theta_v = \pi/4$, at $u_2 = -1.0 \times 10^{-3}$ mm. Regions where $\boldsymbol{\epsilon}^{\mathrm{p}} = \mathbf{0}$ are grayed-out (LI-MA).

Lesson. We can introduce plastic flow non-coaxial to the stress gradient of the yield function through anisotropic regularization!

Strain localization w/ increasing anisotropic regularization effect

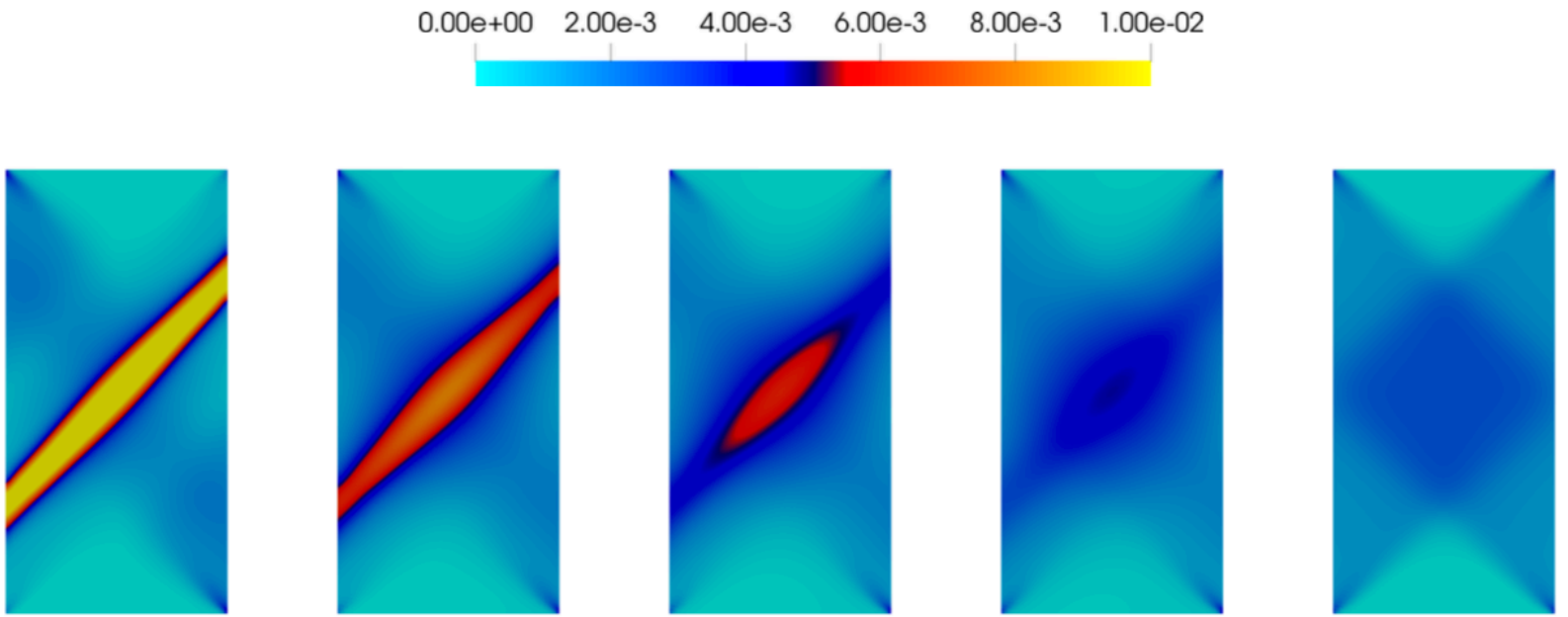

$k_v/k_{v\,0} = 1$ $k_v/k_{v\,0} = 4$ $k_v/k_{v\,0} = 8$ $k_v/k_{v\,0} = 16$ $k_v/k_{v\,0} = 1000$

Fig. 11: Equivalent plastic strain λ for diffusively anisotropic plane strain compression case, with $\phi_v = 16$ and $\boldsymbol{l}_v$ described by $\theta_v = \pi/4$, at $u_2 = -1.0 \times 10^{-3}$ mm (LI-MA).

Boundary Value Problems: Rotation of Microstructural Direction

Anisotropy

In-plane E = 2.4 GPa
Out-of-plane E = 1.4 GPa

β^p = 0.8 [-]

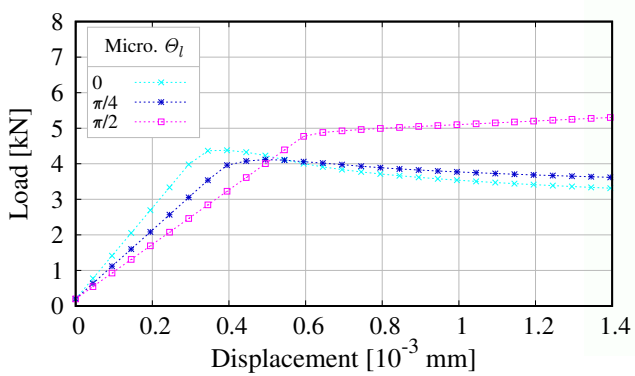

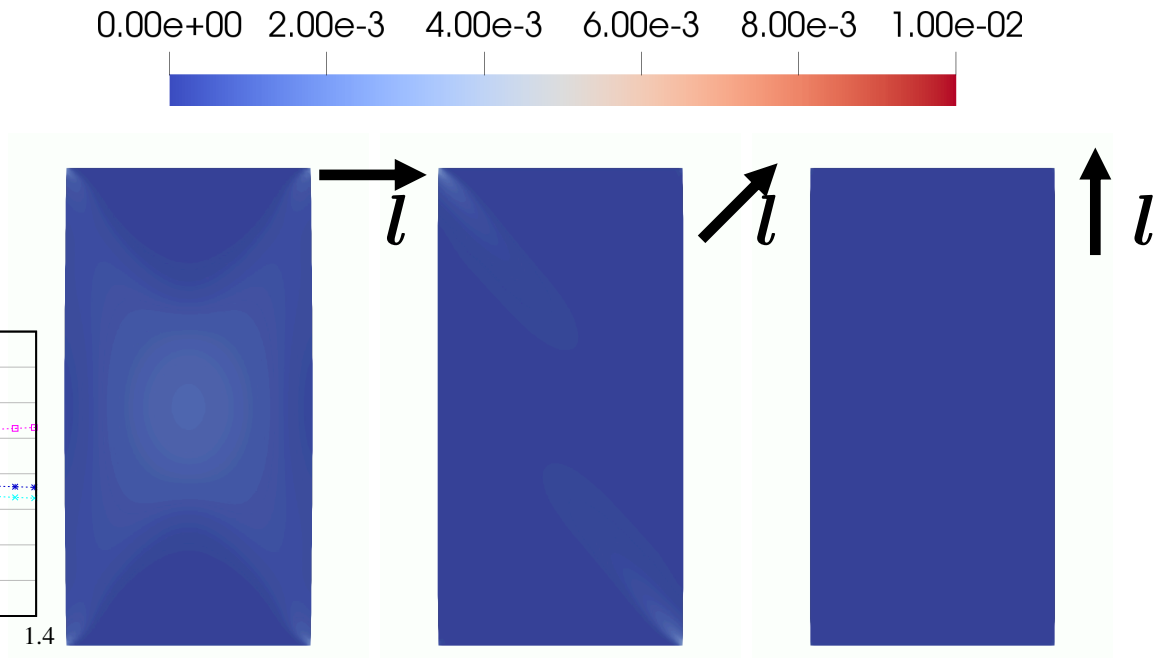

Anisotropic
OCR = 30 [-]
with Softening

Anisotropic
OCR = 30 [-]
with Softening

Anisotropic
OCR = 30 [-]
with Hardening

Micromorphic Regularization of Boundary Value Problems: Isotropic vs. Anisotropic

Anisotropy

In-plane E = 2.4 GPa
Out-of-plane E = 1.4 GPa

β^p = 0.8 [-]

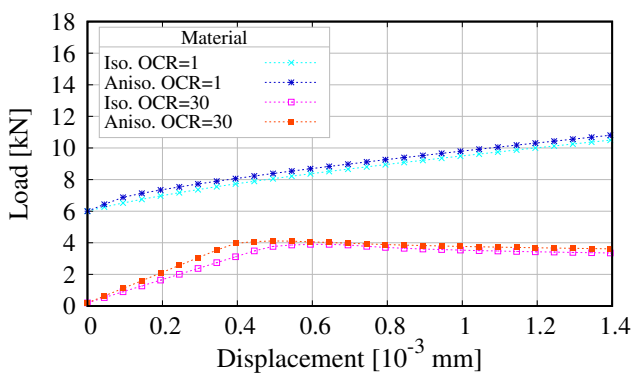

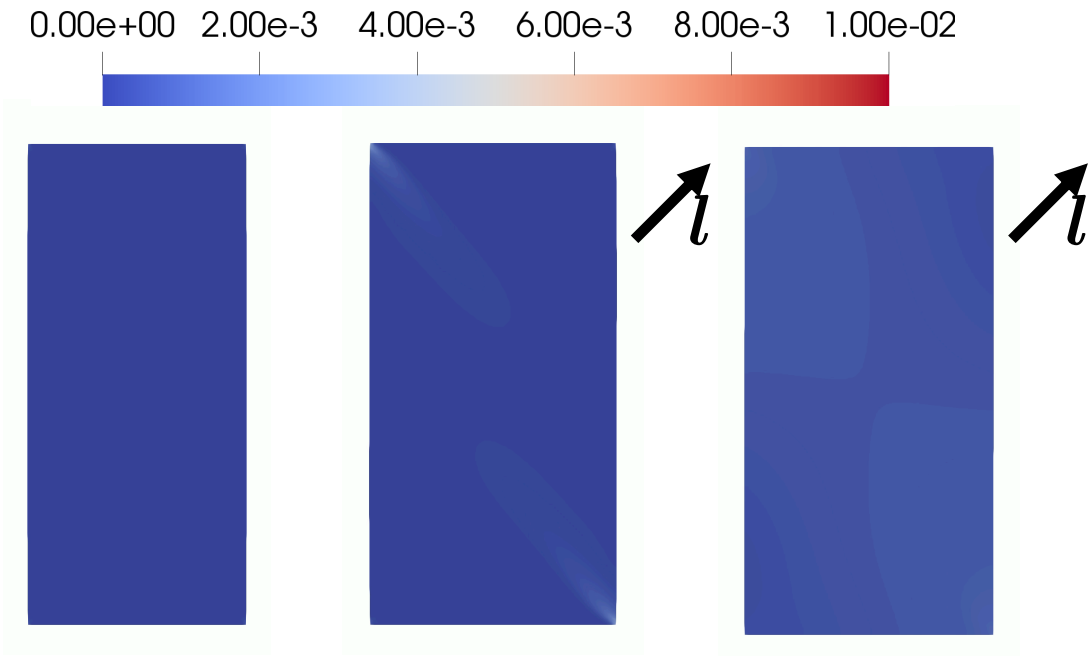

Isotropic
OCR = 30 [-]

Anisotropic
OCR = 30 [-]

Anisotropic
OCR = 1 [-]

Boundary Value Problems: 3D Rotation of Microstructural Direction

Anisotropy

In-plane E = 2.4 GPa
Out-of-plane E = 1.4 GPa

β^p = 0.8 [-]

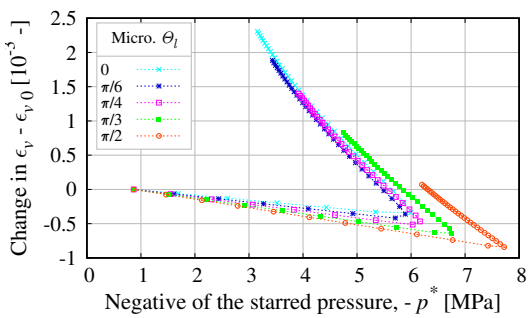

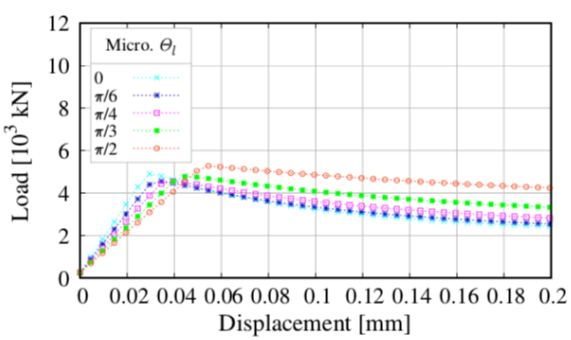

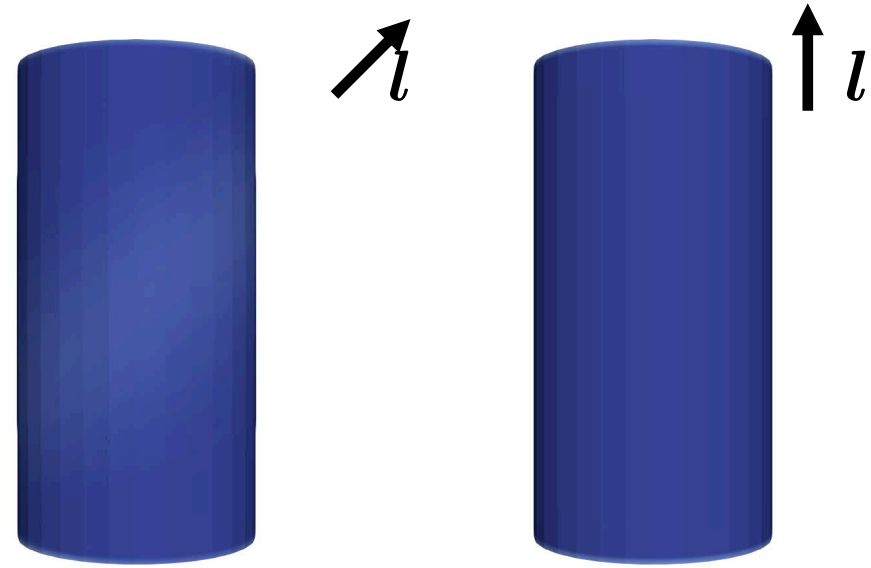

Anisotropic
OCR = 30 [-]
with Softening

Anisotropic
OCR = 30 [-]
with Diffuse Softeniing

Coupled damage-plasticity in crystalline rock

Crystal plasticity theory – Kinematics

- Decomposition of the Total Strain:

$$\boldsymbol{\epsilon} := \nabla^{sym}\boldsymbol{u} = \frac{1}{2}(\nabla\boldsymbol{u} + \nabla^{\mathsf{T}}\boldsymbol{u}) \;\Rightarrow\; \boldsymbol{\epsilon} = \boldsymbol{\epsilon}^{e} + \boldsymbol{\epsilon}^{\theta} + \boldsymbol{\epsilon}^{p} \;\text{ with }\; \boldsymbol{\epsilon}^{p} = \sum_{\alpha}\gamma^{\alpha}\boldsymbol{S}^{\alpha}$$

$\boldsymbol{\epsilon}^{p}$: the integration over all the crystallographic slips

γ^{α}: the plastic slip corresponding to the slip-system α

$\boldsymbol{S}^{\alpha}$: the symmetric part of the *Schmid Tensor* (i.e. $\boldsymbol{s}^{\alpha}\otimes\boldsymbol{m}^{\alpha}$)

$$\boldsymbol{S}^{\alpha} = \frac{1}{2}\left(\boldsymbol{m}^{\alpha}\otimes\boldsymbol{s}^{\alpha} + \boldsymbol{s}^{\alpha}\otimes\boldsymbol{m}^{\alpha}\right)$$

- The Slip-System for Single-Crystal Halite $\{110\}\langle 1\bar{1}0\rangle$ (cf. FCC metal $\{111\}\langle 110\rangle$)

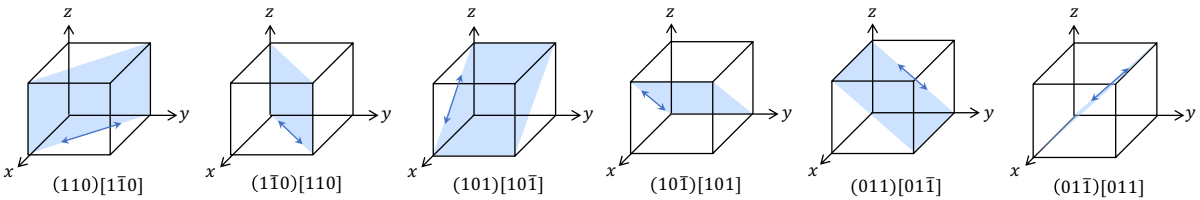

Na & Sun, CMAME 2018

Crystal plasticity theory – Rate Dependence (Creep)

- The stress update algorithm for both rate-dependent and independent behavior
  - Flow rule (viscoplastic regularization)

$$\dot{\gamma}^{\alpha} = C_0 \exp\left(-\frac{Q}{RT}\right)\left[\left(\frac{f^{\alpha+}}{\tau_Y^{\alpha}}+1\right)^{p}-1\right] \quad \text{with} \quad f^{\alpha+} := \begin{cases} f^{\alpha} & \text{if } f^{\alpha} > 0 \\ 0 & \text{otherwise} \end{cases}$$

where β indicates each slip system; C_0 shape factor; Q activation energy; R the gas constant; T temperature; p exponent; f^{α} yield condition; τ_Y^{α} the critical resolved shear stress.

  - The residual and Jacobian matrix (cf. Miehe and Schörder, 2001)

$$r^{\alpha} = \boldsymbol{\sigma} : \boldsymbol{S}^{\alpha} - \tau_Y^{\alpha}\sqrt[p]{\frac{\eta}{\Delta t}\gamma^{\alpha}+1} \quad \text{with} \quad \eta = 1/\left[C_0 \exp\left(-\frac{Q}{RT}\right)\right]$$

$$D^{\alpha\beta} = \boldsymbol{S}^{\alpha} : \mathbb{C}^{e} : \boldsymbol{S}^{\beta} + h\left(\frac{\eta}{\Delta t}\gamma^{\alpha}+1\right)^{1/p} + \tau_Y^{\alpha}\delta^{\alpha\beta}\frac{\eta}{p\Delta t}\left(\frac{\eta}{\Delta t}\gamma^{\alpha}+1\right)^{1/p-1}$$

  - The singular value decomposition (SVD) and pseudo-inverse method are used to regularize the inverse of Jacobian matrix (also see Ultimate algorithm, Borja and Wren, IJNME, 1997).

Anisotropic damage

- **Modeling a single-crystal halite using thermomechanics:**
  - Coupled anisotropic inealsticity and fracture behavior.
  - Rate and temperature dependence – dislocation creep.
  - Intra- and intergranular fracture behavior.
- **Governing equations**
  - Balance of linear momentum

Thermal expansion

$$\nabla \cdot \boldsymbol{\sigma} + \boldsymbol{b} = \mathbf{0} \quad \text{with } \boldsymbol{\sigma} = \frac{\partial \hat{\psi}}{\partial \boldsymbol{\epsilon}^e} = g(\underline{d})\hat{\boldsymbol{\sigma}} \quad \text{with} \quad \hat{\boldsymbol{\sigma}} = \mathbb{C}^e : \boldsymbol{\epsilon}^e - \alpha(\theta - \theta_0)\mathbf{1}$$

Structural heating and plastic dissipation

  - Balance of energy

$$c_v \dot{\theta} = [D_{\text{mech}} - H_\theta] - \nabla \cdot \boldsymbol{q} + r_\theta \quad \text{where} \quad \underbrace{\sum_\alpha (\pi^\alpha \dot{\gamma}^\alpha + g^\alpha \dot{s}^\alpha) + \theta \left(\frac{\partial^2 \hat{\psi}}{\partial \theta \partial \boldsymbol{\epsilon}^e} : \dot{\boldsymbol{\epsilon}}^e \right)}_{D_{\text{mech}} - H_\theta}$$

  - Multiple phase-field equation (microforce balance)

$$2(1 - d_i)\mathcal{H}_i + \frac{G_c}{l} d_i + G_c l \nabla \cdot (\boldsymbol{\omega}_i \cdot \nabla d_i) = 0 \quad \text{with} \quad \mathcal{H}_i = \max_{\tau \in [0,t]} \left\{ \prod_{j \neq i} (1 - d_j)^2 \left[w_+^e + \langle w^p - w_0^p \rangle \right] \right\}$$

Second-order structural tensor(for directional fracture - Knap and Clayton, 2015)

History function for crack propagation and irreversibility (using both thermoelastic and plastic strain energies) – Nguyen et al., 2017

Benchmarks

- **Why we use the multiple phase-field method? How does the method capture anisotropic fracture?**
  - The existing standard FEM code can be easily extended to capture anisotropic damage (without using the higher-order phase-field or constitutive equation).
  - Example: guided crack propagation (cf. Li et al., 2015, Nguyen et al., 2017).

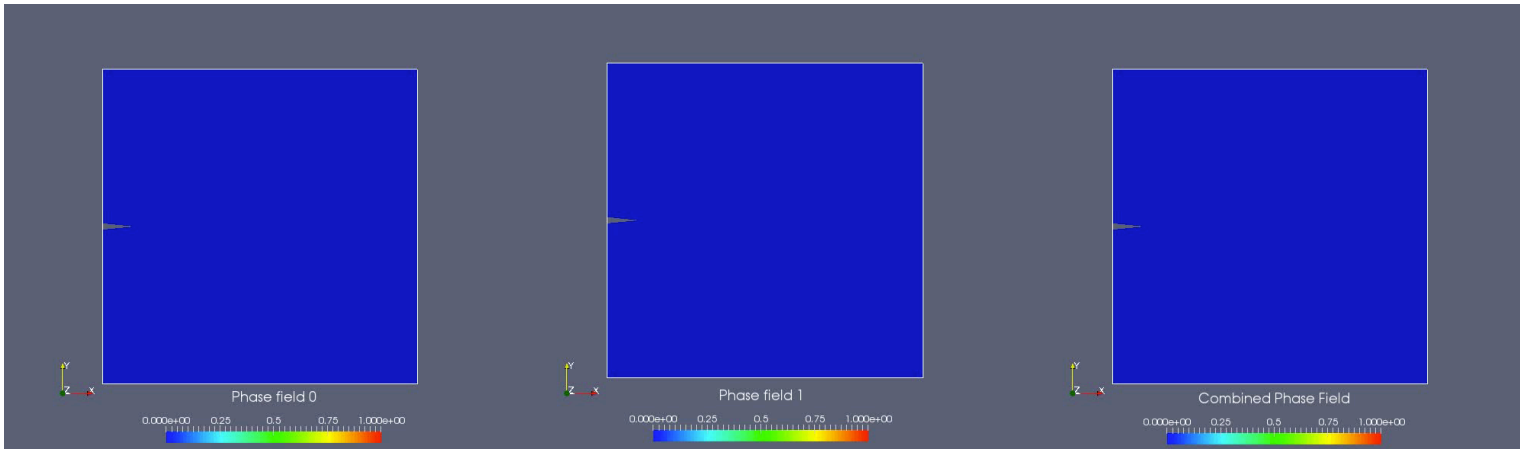

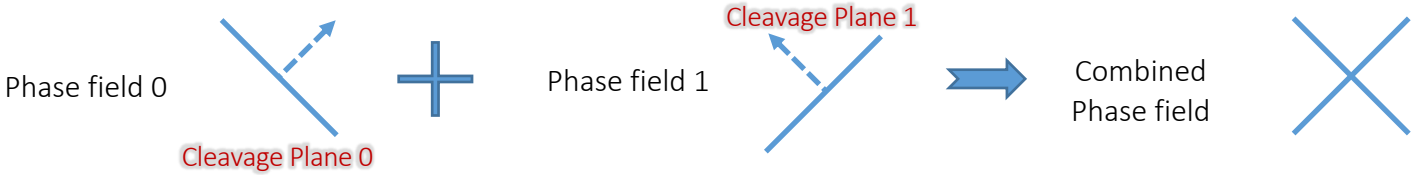

Benchmarks

- **Why we use the multiple phase-field method? How does the method capture anisotropic fracture?**
  - We can relate the number of the slip-system to the number of multiple phase-field variables.
  - This method can be further utilized to model recrystallization.

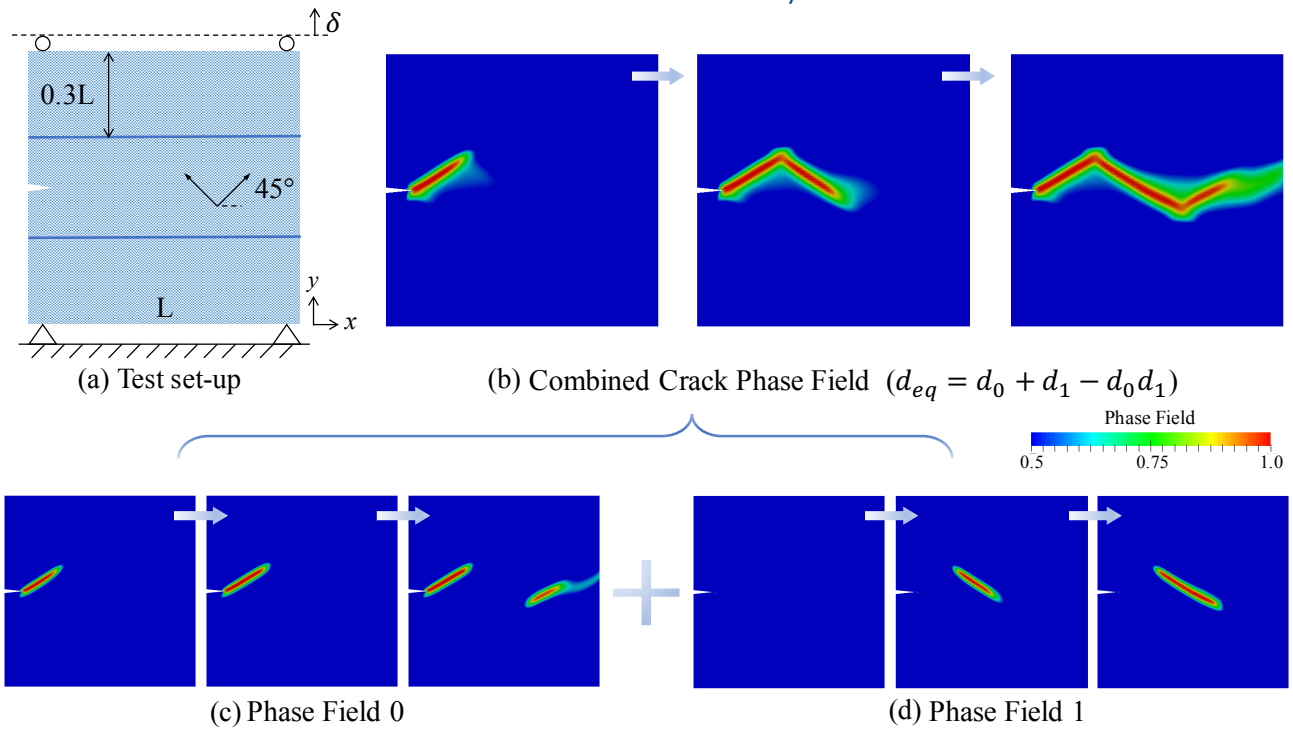

(a) Test set-up

(b) Combined Crack Phase Field $(d_{eq} = d_0 + d_1 - d_0 d_1)$

(c) Phase Field 0

(d) Phase Field 1

Formulations

- **Modeling a single-crystal halite using thermomechanics:**
  - Anisotropic inelastic and fracture behavior.
  - Rate and temperature dependence – dislocation creep.
  - Intra- and intergranular fracture behavior.

- **Governing equations**
  - Balance of linear momentum

Thermal expansion

$$\nabla \cdot \boldsymbol{\sigma} + \boldsymbol{b} = \mathbf{0} \quad \text{with } \boldsymbol{\sigma} = \frac{\partial \hat{\psi}}{\partial \boldsymbol{\epsilon}^e} = g(\underline{d})\hat{\boldsymbol{\sigma}} \quad \text{with} \quad \hat{\boldsymbol{\sigma}} = \mathbb{C}^e : \boldsymbol{\epsilon}^e - \alpha(\theta - \theta_0)\mathbf{1}$$

Structural heating and plastic dissipation

  - Balance of energy

$$c_v \dot{\theta} = [D_{\text{mech}} - H_\theta] - \nabla \cdot \boldsymbol{q} + r_\theta \quad \text{where} \quad \underbrace{\sum_\alpha (\pi^\alpha \dot{\gamma}^\alpha + g^\alpha \dot{s}^\alpha) + \theta \left(\frac{\partial^2 \hat{\psi}}{\partial \theta \partial \boldsymbol{\epsilon}^e} : \dot{\boldsymbol{\epsilon}}^e \right)}_{D_{\text{mech}} - H_\theta}$$

  - Multiple phase-field equation (micro-force balance) (cf. Gurtin 1996, Na & Sun, 2017, Choo & Sun, 2018a,b).

$$2(1 - d_i)\mathcal{H}_i + \frac{G_c}{l} d_i + G_c l \nabla \cdot (\boldsymbol{\omega}_i \cdot \nabla d_i) = 0 \quad \text{with} \quad \mathcal{H}_i = \max_{\tau \in [0,t]} \left\{ \prod_{j \neq i} (1 - d_j)^2 \left[w_+^e + \langle w^p - w_0^p \rangle \right] \right\}$$

a second-order structural tensor (for directional fracture)

History function for crack propagation and irreversibility (using both thermoelastic and plastic strain energies)

Formulations

- **How is each balance equation related?**
  - A combined stored energy functional

$$\psi = \hat{\psi}^e(\boldsymbol{\epsilon}^e, \theta, \underline{d}) + \hat{\psi}^p(\underline{s}, \underline{d}) + \hat{\psi}^c(\underline{d}, \nabla \underline{d}, \underline{\omega}) + \hat{\psi}^\theta(\theta)$$

Thermoelastic strain energy

$$\hat{\psi}^e(\boldsymbol{\epsilon}^e, \theta, \underline{d}) = g(\underline{d}) w^e(\boldsymbol{\epsilon}^e, \theta) \quad \text{with} \quad w^e(\boldsymbol{\epsilon}^e, \theta) = \frac{1}{2}\boldsymbol{\epsilon}^e : \mathbb{C}^e : \boldsymbol{\epsilon}^e - \alpha(\theta - \theta_0)\,\mathrm{tr}\,\boldsymbol{\epsilon}^e$$

Plastic strain energy

$$\hat{\psi}^p(\underline{s}, \underline{d}) = g(\underline{d})^p \langle w^p - w_0^p \rangle, \text{ with } g(\underline{d})^p = g(\underline{d}) \text{ and } w^p = \frac{1}{2}\sum_\alpha h(s^\alpha)^2$$

Total crack surface energy

$$\hat{\psi}^c = G_c \sum_i \left[\frac{1}{2l}(d_i)^2 + \frac{l}{2}\boldsymbol{\omega}_i : (\nabla d_i \otimes \nabla d_i) \right]$$

Purely thermal energy for heat transfer

$$\hat{\psi}^\theta = c_v \left[(\theta - \theta_0) - \theta \ln(\theta/\theta_0) \right]$$

Applications

Modeling a single-crystal halite using thermomechanics:

Anisotropic inelasticity & fracture | Temperature dependence | Rate dependence | Intra- and inter granular fracture

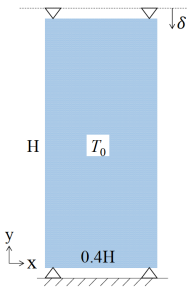

<Test set-up>

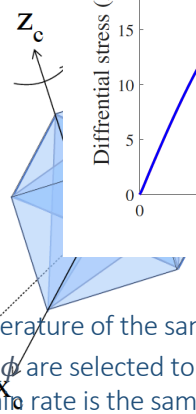

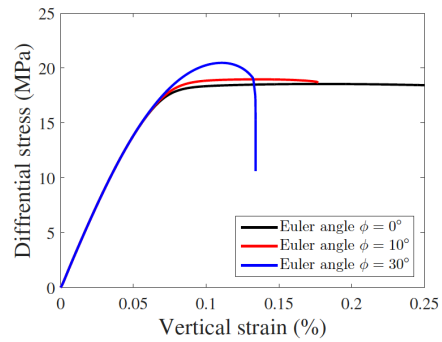

< Definition of Euler angle: ϕ, θ >

- ✓ The initial temperature of the sample domain is fixed with 25°.
- ✓ Three different ϕ are selected to change the orientation of the slip system (strain rate is the same as 1.0E-5/sec.).
- ✓ Changing orientations of the slip systems induces different mechanical responses (stress-strain) along with different patterns of damage and plastic slip.

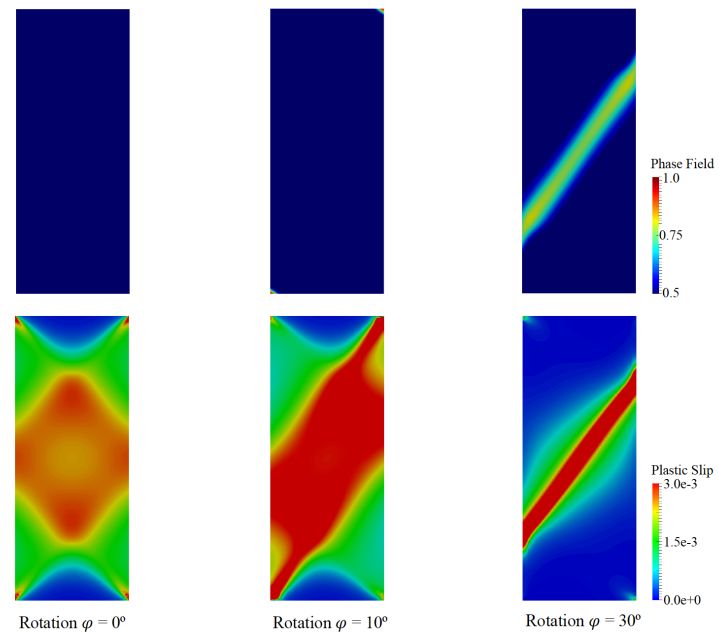

Note: θ is fixed with 0°

Applications

Modeling a single-crystal halite using thermomechanics:

Anisotropic inelasticity & fracture | Temperature dependence | Rate dependence | Intra- and inter granular fracture

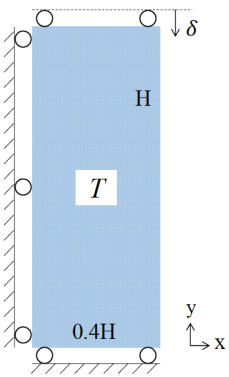

<Test set-up>

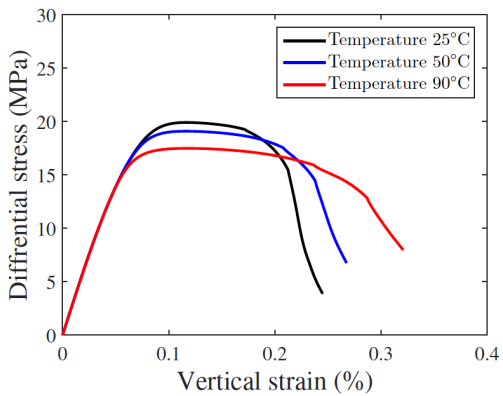

- ✓ Three initial temperatures of the sample domain are selected to analyze the thermal impact on mechanical responses.
- ✓ As the temperature increases, the more ductile behavior is obtained from stress-stress curves.
- ✓ The thermal dissipation suppresses the crack propagation and leads to different plastic patterns.

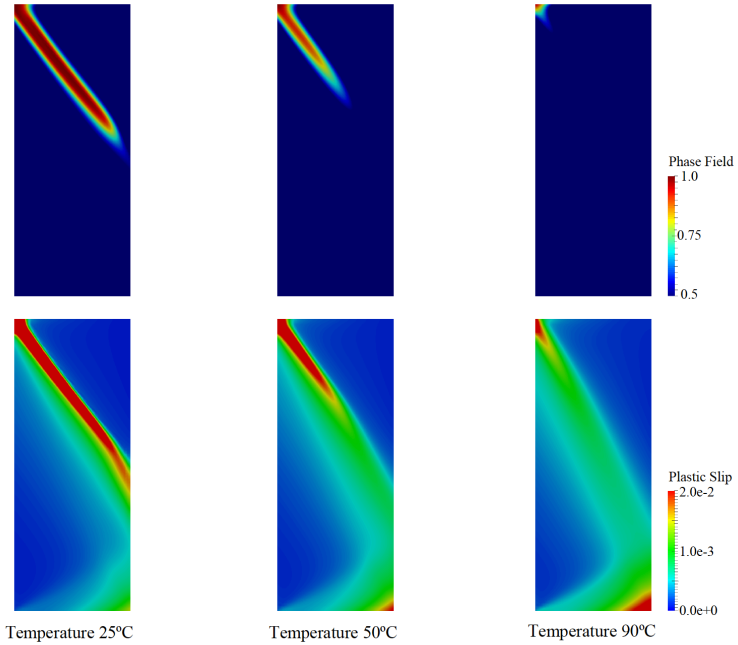

Note: The results are captured at the same vertical strain level (0.24%), and Euler angles are fixed for all cases: θ = 0º and ϕ = 70º

Modeling a single-crystal halite in 3D

- All the slip-systems associated with each crack phase-field (different orientations)

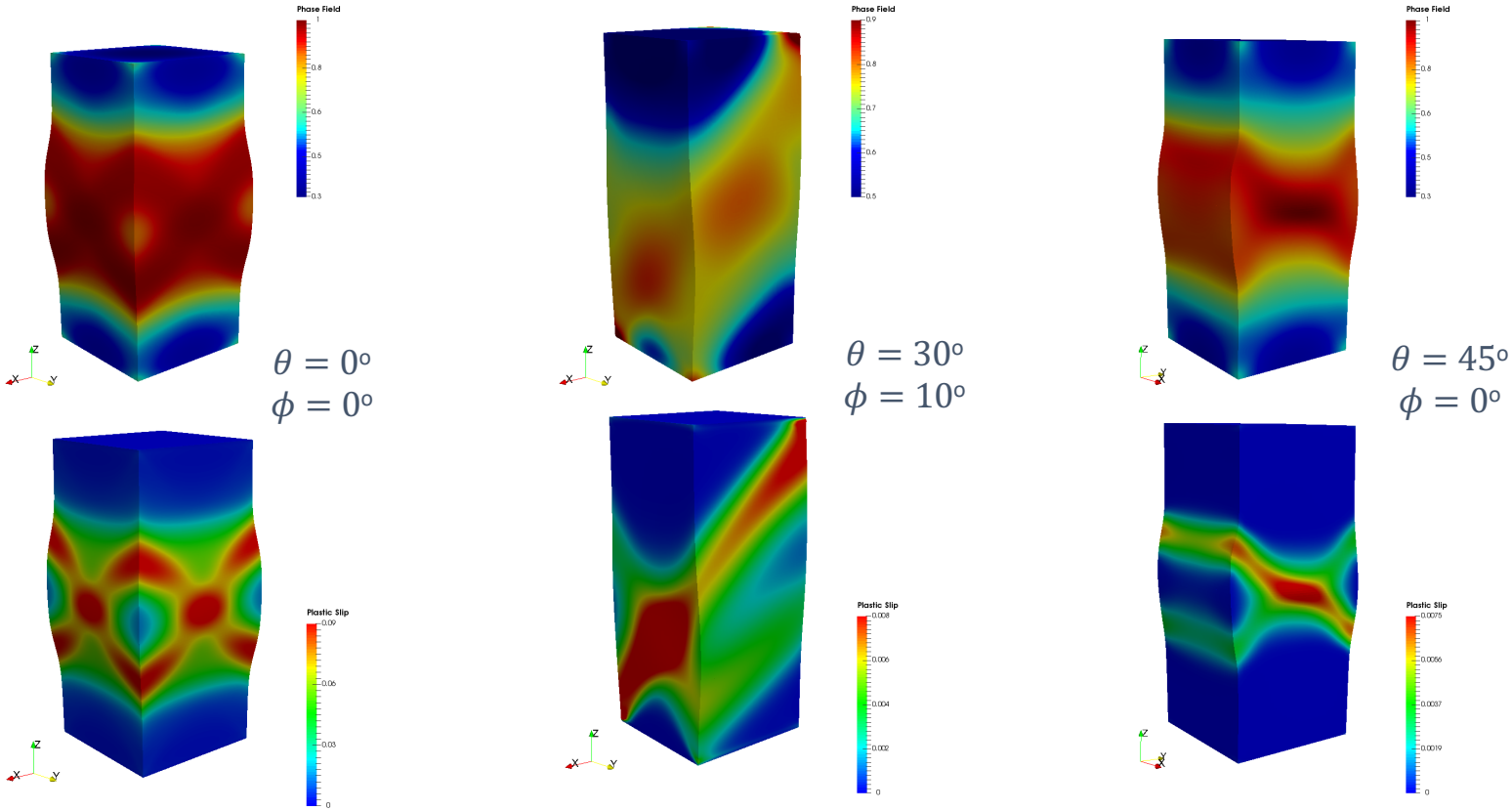

Strongly Anisotropic materials in the brittle regime

FFT-based High-order Phase-field

Regularized cleavage surface energy for multi-phase-field

$$\gamma\left(d, \nabla d, \nabla^2 d\right) = \frac{1}{2l_0}d^2 + \frac{l_0}{4}\nabla d \cdot \nabla d + \frac{l_0^3}{32}\nabla^2 d : \mathbb{A} : \nabla^2 d + \frac{1}{2}\beta_1 \left(d-1\right)^2$$

Cleavage energy anisotropy

Initial phase field penalization

First order variation, integration by part twice

$$\int_\Omega \left[2\left(d-1\right)\mathcal{H}_1^1 + \frac{G_c}{l_0}d - \nabla \cdot \left(\frac{G_c l_0}{2}\nabla d\right) + \nabla^2 : \left(\frac{G_c l_0^3}{16}\mathbb{A} : \nabla^2 d\right) + \beta_1\left(d-1\right)\right]\delta d \mathrm{d}\Omega$$
$$+ \underbrace{\int_{\partial\Omega}\left[\frac{G_c l_0}{2}\nabla d \cdot \vec{n} + \frac{G_c l_0^3}{16}\nabla^2 d : \mathbb{A} : \left(\nabla \delta d \otimes \vec{n}\right) - \frac{G_c l_0^3}{16}\nabla \cdot \left(\mathbb{A} : \nabla^2 d\right) \cdot \vec{n}\delta d\right]\mathrm{d}S}_{\text{Surface integral over periodic RVE}} = 0.$$

Assumptions:

1) A, G_c and l_0 are periodic → surface integral vanishes
2) A, G_c are piecewise constant, l_0 is constant → grad(A) = 0

$$\left(2\psi_1^1 + \frac{G_c}{l_0} + \frac{G_c l_0}{2}\mathcal{F}^{-1}\xi \cdot \xi\mathcal{F} + \frac{G_c l_0^3}{16}\mathbb{A} :: \mathcal{F}^{-1}\xi \otimes \xi \otimes \xi \otimes \xi\mathcal{F} + \beta\right) d = 2\psi_1^1 + \beta.$$

Ma & Sun, under review

Numerical Examples (1D rod)

d

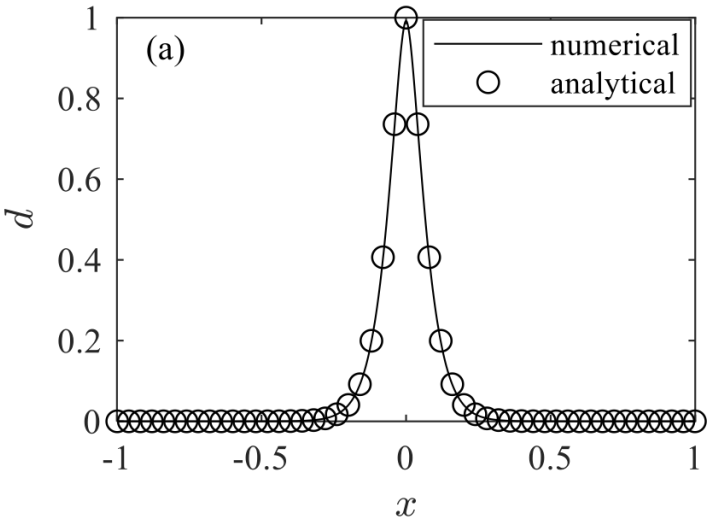

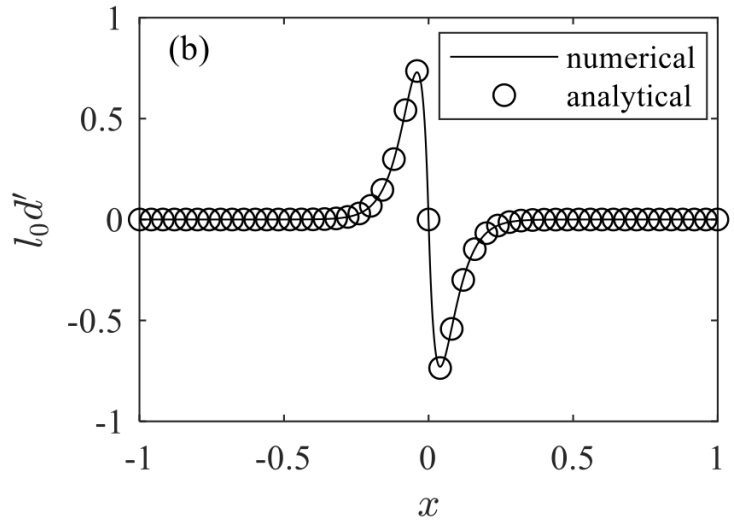

∇d

$\nabla^2 d$

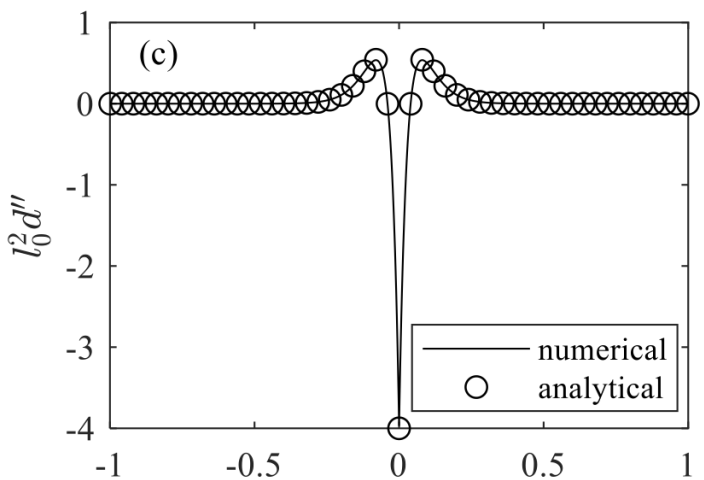

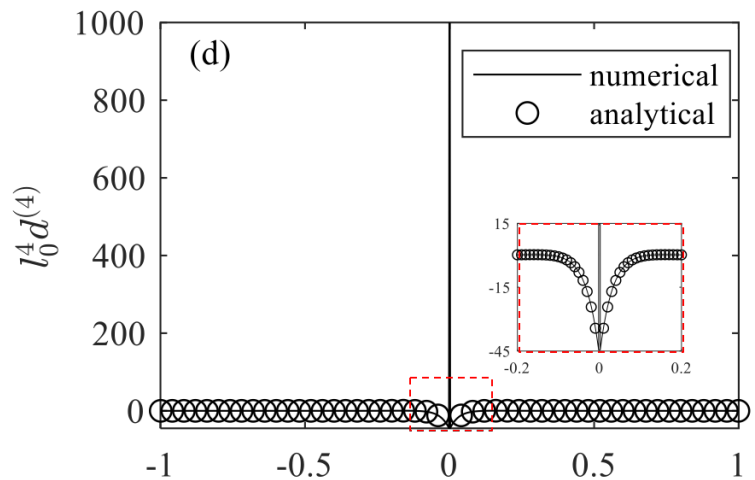

$\nabla^4 d$

- trigonometric polynomials accurately calculate high order gradient without spurious oscillations
- Gibbs effect is dampened by using finite difference based frequency vectors

Numerical Accuracy and Efficiency of FFT-based method

Gibbs effect

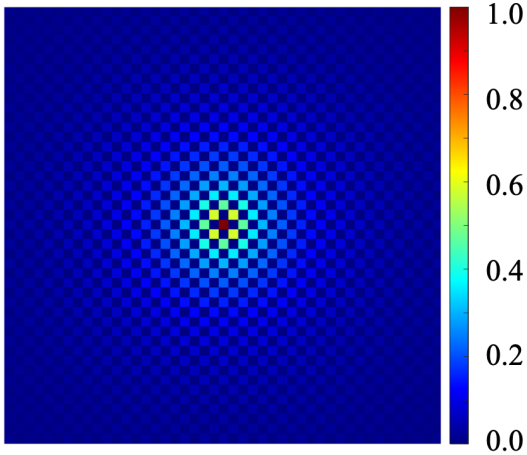

w/ Gibbs effect

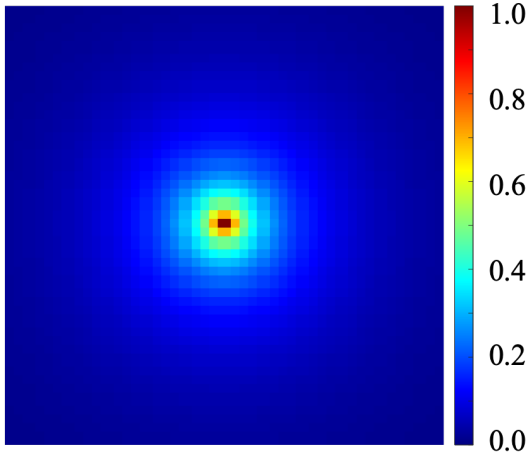

w/o Gibbs effect

Numerical Efficiency

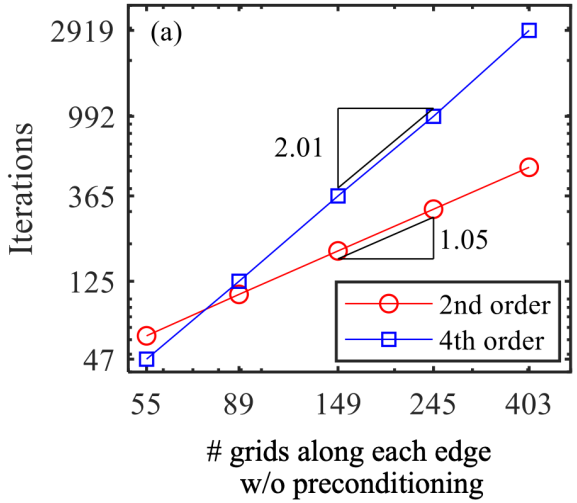

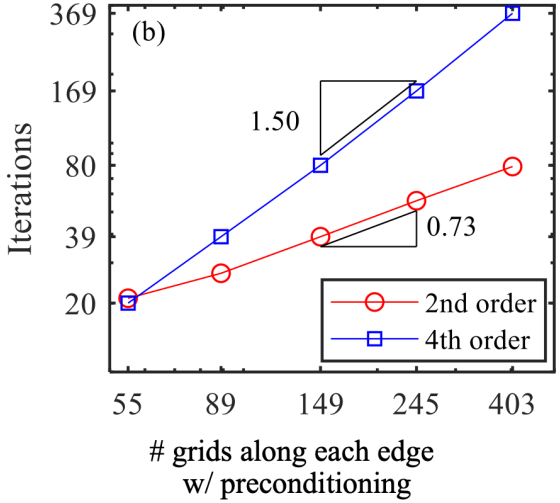

Observation:

- high-order phase-field more expensive than multi-phase-field
- preconditioning matrix is effective in accelerating the iterative linear solver

Numerical Examples (3D polycrystalline rock salt)

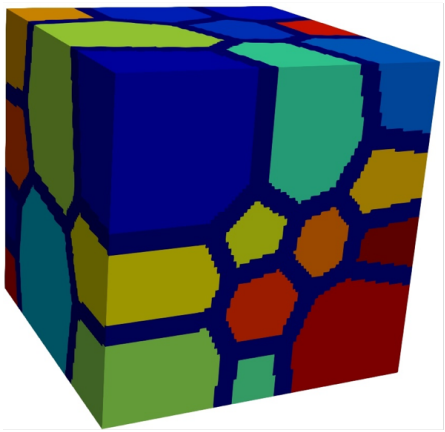

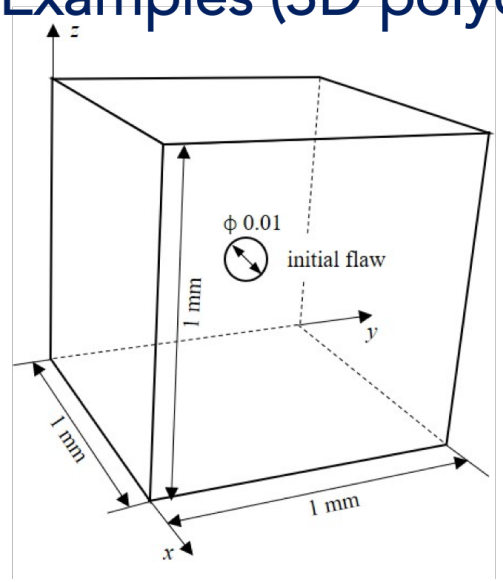

Material:
- 3D polycrystalline rock salt
- 40 grains with random initial orientation
- 101^3 Fourier grid points

Load case:
- Uniaxial tension of RVE with central flaw

Constitutive:
- mechanical: small strain elasticity
- phase field: strongly anisotropy

Multi-phase-field (MPM)

High-order phase-field (HPM)

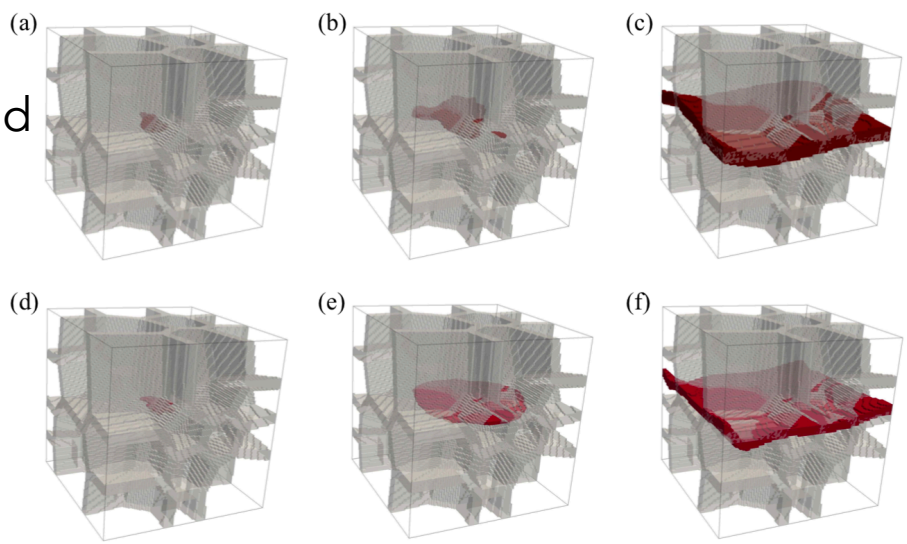

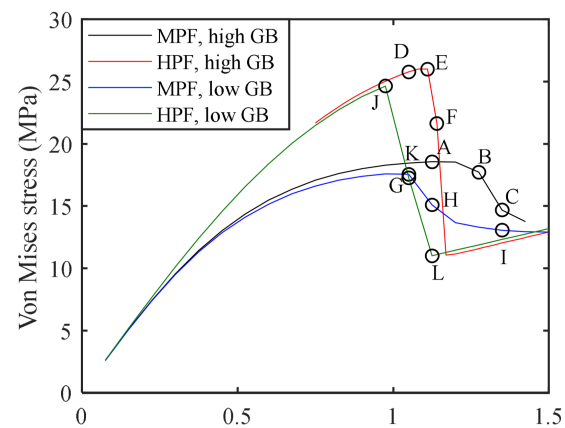

Sawtooth crack pattern in strongly anisotropic phase field fracture model

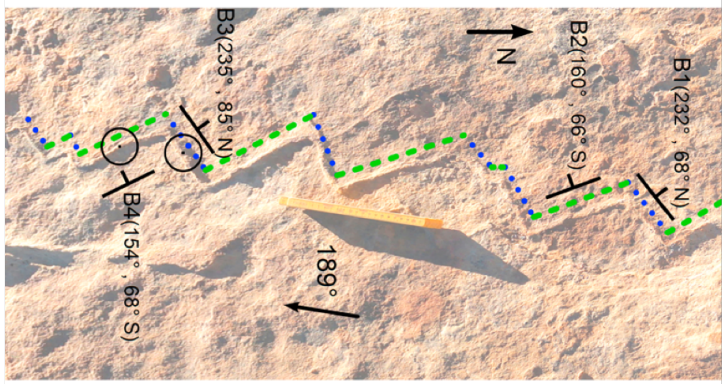

<Outcrop of wiggly compaction bands (from Liu et al., 2015)>

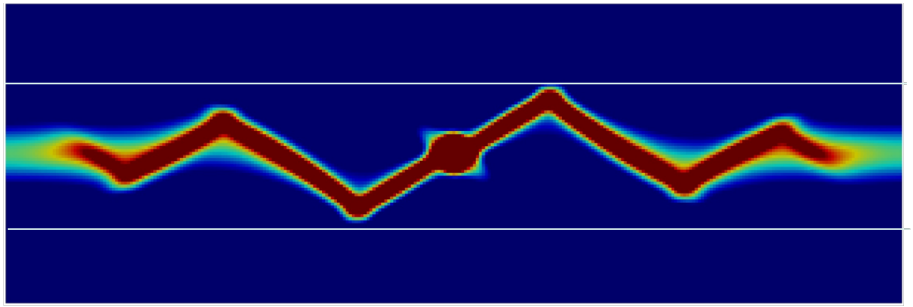

$$d = 1 - (1 - d_1)(1 - d_2)$$

multi-phase-field

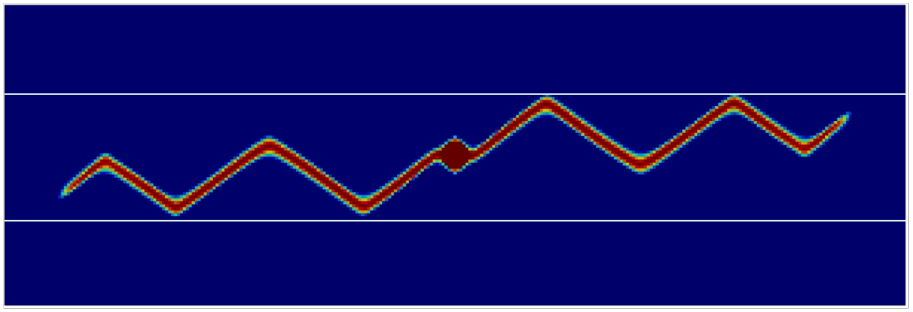

high-order phase-field

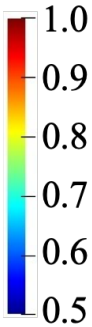

Observations

- Both multi-phase-field and high-order phase-field can capture the sawtooth crack pattern
- Multi-phase-field is more regularized
- Difference between MPF and HPF is caused by numerical parameters

Fracture healing and precipitating creeping

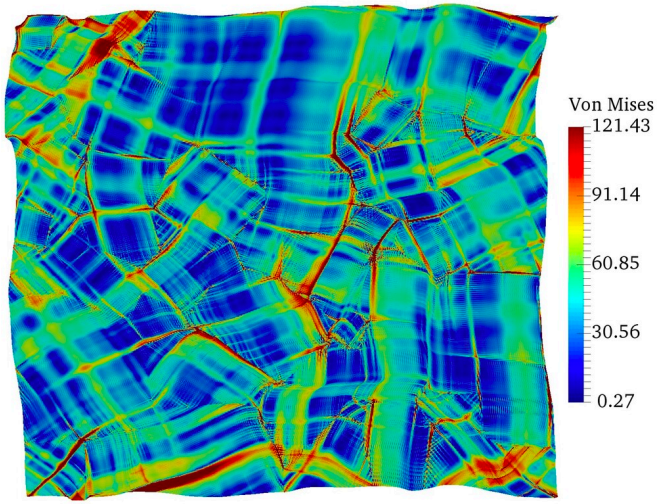

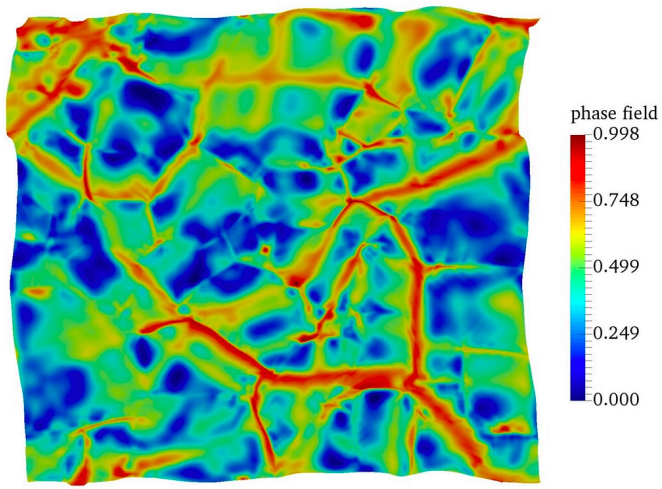

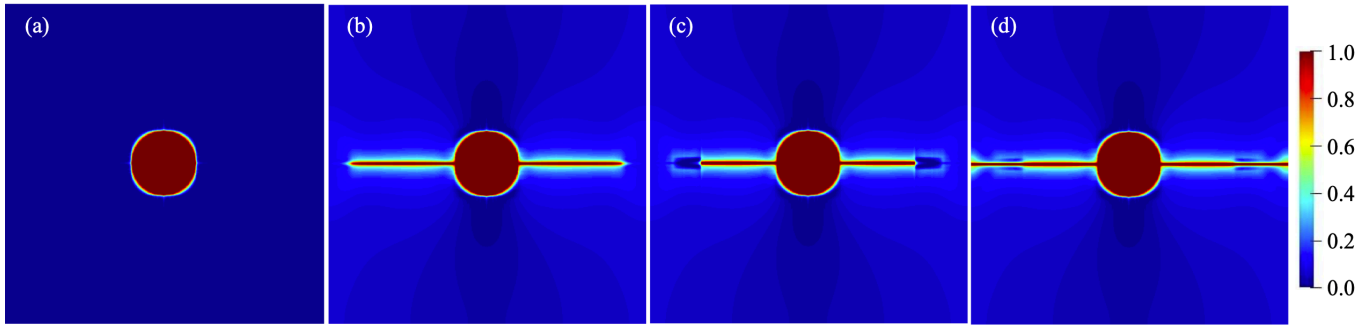

Acknowledgements

- Army Research Office: Young Investigator Program Award
- Air Force Office of Scientific Research, Young Investigator Program Award
- National Science Foundation: EAR-1516300 and CMMI-1445033
- Sandia National Laboratories
- US Department of Energy Office of Nuclear Energy
- Columbia University

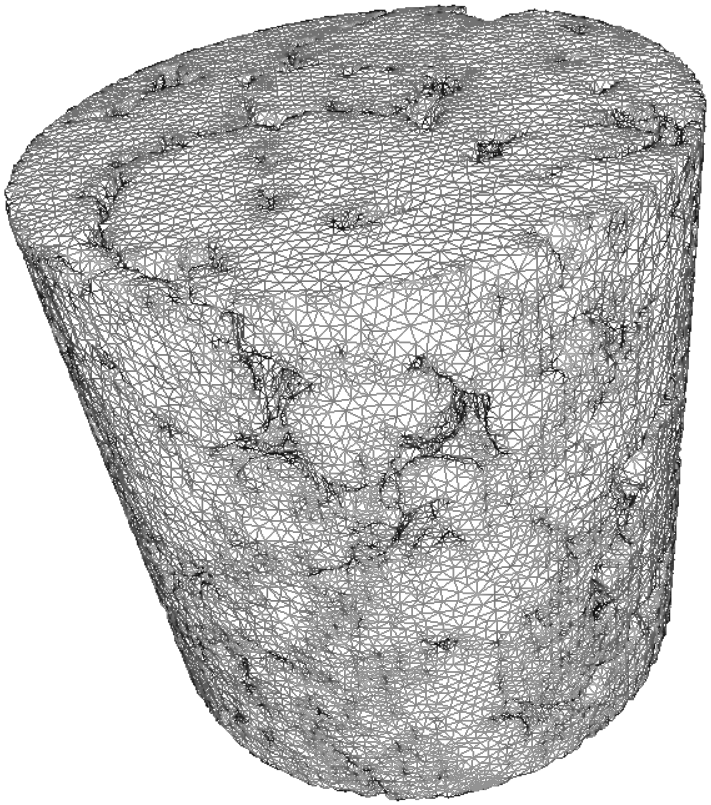

THANK YOU!

More information can be found at
www.poromehanics.org